NASA-CR-152, 125

FINAL TECHNICAL REPORT

CONTINUED DEVELOPMENT OF DOPED-GERMANIUM PHOTOCONDUCTORS FOR ASTRONOMICAL OBSERVATIONS AT WAVELENGTHS FROM 30 TO 120 MICROMETERS

Contract No. NAS2-9599

For - National Aeronautics and Space Administration
Ames Research Center
Moffett Field, CA 94035

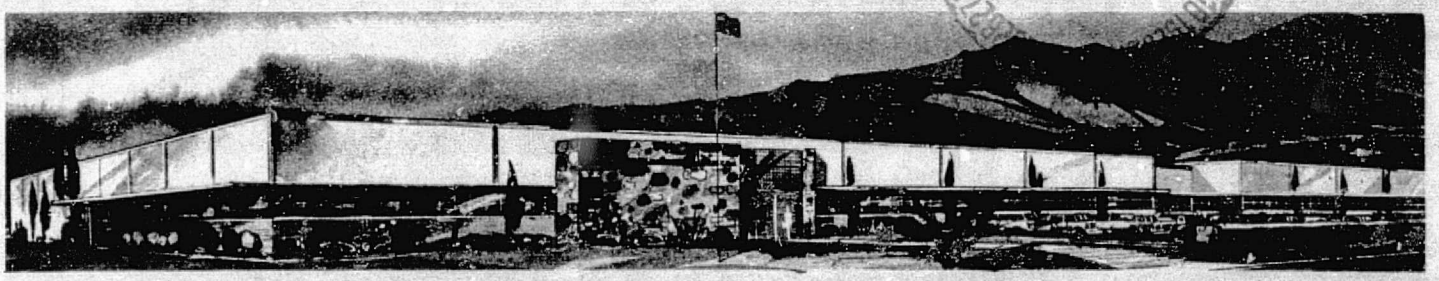

SANTA BARBARA RESEARCH CENTER
A Subsidiary of Hughes Aircraft Company
SBRC

SANTA BARBARA RESEARCH CENTER

A Subsidiary of Hughes Aircraft Company

75 COROMAR DRIVE, GOLETA, CALIFORNIA

FINAL TECHNICAL REPORT

CONTINUED DEVELOPMENT OF DOPED-GERMANIUM PHOTOCONDUCTORS FOR ASTRONOMICAL OBSERVATIONS AT WAVELENGTHS FROM 30 TO 120 MICROMETERS

Contract No. NAS2-9599

For

National Aeronautics and Space Administration
Ames Research Center
Moffett Field, CA 94035

24 April 1978

Prepared by P.R. Bratt
P. R. Bratt
Senior Scientist

Prepared by L.E. Long for
N. N. Lewis
Project Engineer

Prepared and Approved by L.E. Long
L. E. Long
Project Manager

PREFACE

This report describes the results of a technology development program directed toward the optimization of the performance of beryllium-doped germanium (Ge:Be) and gallium-doped germanium (Ge:Ga) infrared detectors operating near 3°K at low backgrounds (10^8 photons/sec/cm^2) and low frequencies (≥ 0.05 Hz). The work was performed at the Santa Barbara Research Center over the period from 27 May 1977 to 12 April 1978.

The Project Manager for the program was Lawrence E. Long. The Project Engineer was Nancy N. Lewis. The Project Technical Monitor for NASA/Ames was Craig McCreight. A number of other people at SBRC made significant contributions to this project. Roger A. Cole and Eugene D. Van Orsdell grew the Ge:Ga and Ge:Be crystals. David J. Calhoun and James B. Knutsen made the Hall effect measurements and data analysis. Beulah L. Marolf fabricated detectors, and Courtney W. Manker and Fred J. Strobach assisted in the design and assembly of the low-background test fixtures. Most of the testing was done by James M. Fulton. Richard L. Nielsen and H. Andrew Graham provided valuable assistance in trouble shooting test problems and evaluation of test results.

CONTENTS

Section 1
INTRODUCTION AND SUMMARY

The work described in this report was a continuation of a previous technology development program on Ge:Be and Ge:Ga detectors funded by NASA/Goddard and administered by Kitt Peak National Observatory; and is a direct follow-on of work performed under NASA/ARC contract NAS2-9385. During the first phase of this work, emphasis was on Ge:Ga detector development. During the second phase, more emphasis was placed on Ge:Be detector development. The ultimate goal was to develop the technology for production of doped-germanium detectors which have optimized performance in the 30- to 120-μm wavelength range and are capable of achieving the objectives of the Infrared Astronomical Satellite (IRAS) space mission. Because of the short duration of the NAS2-9385 contract, the technology for producing fully optimized detectors was not fully developed, although significant advances were made.

The current contract was funded to continue this work, with the same ultimate goal. The work on this phase was divided into the following major tasks:

1. Growth of Ge:Ga crystals from high-purity starting material with Ga concentrations of 4 and 8 x 10^{14} atoms/cc or higher using the zone leveling method developed on the previous program to produce a uniform Ga doping concentration.
2. Growth of a Ge:Ga crystal with a Ga concentration of 1 to 2 x 10^{14} atoms/cm^3.
3. Growth of uncompensated Ge:Be crystals from high-purity starting material with a range of Be concentrations between 1 and 2 x 10^{15} atoms/cm^3.
4. Growth of Ge:Be crystals using intentionally compensated starting material.
5. Evaluation of crystals by means of Hall effect and resistance measurements as a function of temperature.

6. Fabrication and test of detectors made from both Ge:Be and Ge:Ga crystals to determine the relative performance between different crystals. Correlation of detector test data with material evaluation data and analysis of how to further optimize detector performance.

Since the refining and doping techniques for Ge:Ga material were well under control, one Ge:Ga crystal was grown immediately at the onset of the program. The major emphasis after that point was concentrated on the Ge:Be work. With the problems encountered during the Ge:Be crystal growth, and with limited funding, it became evident that the Ge:Ga effort would have to be curtailed; no more Ge:Ga crystals were grown.

Seven Ge:Be crystals were grown in the attempt to optimize the dopant levels and perfect the growth and doping techniques. Four of the seven were grown using compensated material. The compensation level in three of these was lower than expected, however.

Although not all of the tasks defined at the outset of the program were performed, the major objectives were achieved. The results of this phase may be summarized as follows:

The zone leveling technique for growing Ge:Ga crystals continued to show that a method had been established for producing uniform material to the desired concentration.

The results of the Ge:Ga crystal that was grown showed that the dopant concentration used on the last phase of the program was closer to optimum than on this phase.

Although the detectors manufactured from the Ge:Ga crystal were low in performance, the detector fabrication technology was consistent and is adequate for fabrication of large focal plane arrays.

Techniques for doping the Ge:Be material were brought under control, although several crystals were grown to achieve this. The last few crystals were uniformly doped over large sections of the crystal.

Detector fabrication techniques for Ge:Be were also consistent, yielding several detectors of good quality. Fabrication techniques are adequate for large focal plane arrays.

Section 2
REVIEW OF PREVIOUS WORK

Previous work involved exploratory development in Ge:Ga crystal growth as well as detector fabrication technology using both Ge:Ga and Ge:Be material. On the first phase of this work, Ge:Ga detectors were made from material furnished by the Naval Research Laboratories (W. J. Moore) and from material produced at SBRC. Ge:Be detectors were made only from material furnished by NRL. The results of the Ge:Ga work were very encouraging in that the crystal growth method used was shown to be capable of producing a specified Ga doping concentration with very low concentrations of residual donor impurities. Detector performance was found to be reasonably good with NEP = 4×10^{-16} watt/Hz$^{\frac{1}{2}}$ at 100 μm for a background flux of 1.8×10^{10} photons/sec/cm^2, and 1.3×10^{-16} watt/Hz$^{\frac{1}{2}}$ for a background flux of 1.2×10^{9} photons/sec/cm^2. The Ge:Be detectors made from NRL material achieved an NEP of 1×10^{-15} watts/Hz$^{\frac{1}{2}}$ at 40 μm with a background flux of 1.9×10^{9} photons/sec/cm^2.

This work clearly demonstrated the feasibility of these detector materials as very sensitive detectors of long-wavelength radiation under low-temperature and low-background conditions of operation. It established a starting point from which further technology development efforts could proceed, and fostered a confidence that the ultimate performance goals could be realized within reasonable time and cost constraints.

The zone melting method for growth of Ge:Ga crystals was implemented and found to work well. After growth of a few crystals, it was realized that a more uniform Ga doping concentration should be attainable by going to a zone leveling modification using the same furnace. This became one of the primary tasks for the next phase of the work. The zone leveling technique for growing Ge:Ga crystals was implemented and shown to produce a uniform Ga doping concentration over more than 5 inches of ingot length. This

established a reliable material production method which yielded a quantity of detector material more than adequate for the IRAS focal plane array (FPA) fabrication. The growth and evaluation of the Ge:Ga crystal is covered in the final report for that program[1].

No previous experience with the growth of Ge:Be crystals existed at SBRC prior to the start of contract NAS2-9385. The determination and perfection of the crystal growing methods therefore became a major new task. Growth of Ge:Be crystals proved to be difficult because of small amounts of oxygen in the zone melting furnace which either formed a Be-O compound on the surface of the ingot or a Be-O complex inside the ingot. In either case, Be is effectively removed to an inactive site and cannot produce impurity photoconductivity. The problem was solved by growing Ge:Be crystals under vacuum. This yielded a small amount of material for detector test and evaluation; however, uniformly doped Ge:Be ingots were not obtained, and the control of Be doping concentration was not as good as for Ga doping. Further work on the Ge:Be crystal growth technology was warranted, and was continued in the current program, as reported herein.

Detector fabrication technology which had been previously developed at SBRC for doped Ge detectors was found to work well on these longer wavelength materials. In particular, the use of ion implantation in the formation of electrical contacts to the crystals was shown to give an ohmic contact with little or no excess noise for frequencies down to 1 Hz.

The fundamental principles of operation of a doped-germanium far infrared detector were described in the Final Technical Report for the first phase of this program[2]. The detector operates as an extrinsic photoconductor. Photoionization of the doping impurity atoms (Ga or Be) by infrared radiation

1. P. R. Bratt and N. N. Lewis, "Development of Doped Germanium Photoconductors for Astronomical Observations at Wavelengths from 30 to 120 Micrometers", Final Technical Report, Contract NAS2-9385, Santa Barbara Research Center, 30 November 1977 (NASA-CR-152, 046)

2. P. R. Bratt, "Improved Ge:Ga and Ge:Be Far Infrared Detector Development," Final Technical Report, Contract No. 86310 (AURA), Santa Barbara Research Center, October 1977

produces extra free holes in the crystal which increase its conductivity. This conductivity increase can be easily measured using a suitable electrical circuit.

The energy required for ionization of the Ga atoms in Ge is 0.011 eV. Thus, incoming photons with an energy greater than this value can cause photoionization; those with a lesser energy cannot. This requirement can be expressed in terms of the infrared photon's wavelength as follows:

$$\frac{hc}{\lambda} \geq \epsilon_i \qquad (1)$$

where h is Planck's constant, c the speed of light, λ is the wavelength, and ϵ_i is the ionization energy. For energies expressed in eV and wavelength in μm, Equation (1) can be rewritten as

$$\lambda \leq \frac{1.24}{\epsilon_i} \qquad (2)$$

Thus, photons of wavelength less than 100 μm can produce photoconductivity in Ge:Ga crystals. The Be atom in Ge has an ionization energy of 0.024 eV. Therefore, photons of wavelength less than 52 μm can produce photoconductivity in Ge:Be crystals.

The optimization of a detector's sensitivity involves an attempt to maximize the photoconductive response and minimize the various noise sources present either in the detector itself or in the associated electrical components.

A theoretical analysis of detector operation under low background conditions has pointed out the directions in which to proceed toward optimization of detector performance. These may be summarized as follows:

1. Grow Ge:Ga and Ge:Be crystals with doping concentrations as large as possible so as to maximize the responsive quantum efficiency, but keep the doping concentration below the point where impurity hopping conductivity begins to significantly lower detector resistance. This implies that there is some optimum doping concentration which will be different for each type of impurity atom. This concentration must be determined experimentally for the particular temperatures of operation and background photon flux levels expected in the IRAS mission.

2. Maximize the photoconductive gain of the detector by using material with long free-hole lifetime. This mandates the use of high-purity Ge starting material with a very low concentration of residual donor impurities. Fabricate detector crystals with a minimum interelectrode spacing and operate with applied electric field strength as large as possible.

3. Provide electrical contacts to the doped Ge crystal which do not produce excess noise and are "ohmic" for transport of charge carriers (free holes) into and out of the crystal.

These guidelines formed the basis for the development efforts that were carried out in the two NASA programs, the latter being covered in this report.

Section 3
Ge:Ga CRYSTAL GROWTH AND EVALUATION

CRYSTAL GROWTH

One Ge:Ga crystal was grown during this phase of the program. The crystal was doped to two levels in different zones of the crystal: 5×10^{14} and 8×10^{14} atoms/cm^3. The doping concentration was higher than that of the previous crystal to see if material with a higher responsivity and impact ionization level could be obtained.

The method of Ge purification by multipass zone refining described in the first report was used[3]. Ga doping by means of pellet dropping spoons was also used. The crystal grown contains over 4 inches of material in the central region of the ingot, doped relatively uniformly to two levels in two zones. The seed end was subsequently cut off for reuse and the tail end was cut off and discarded as scrap.

DOPING CONCENTRATION

Samples were cut from the doped region at 1-inch intervals for evaluation by Hall effect measurements. The Ga doping concentration was found to be as expected within the 4-inch length which was evaluated. The results are shown in Figure 3-1. This provided high quality detector material with a doping concentration 2 to 3 times greater than that used in our previous work.

Evaluation of selected samples by means of Hall effect measurements versus temperature was also done. Comparison of experimental data points with theoretically generated curves provides a determination of the residual donor atom concentration in the crystal. Details of the method of analysis

---

3. Ibid.

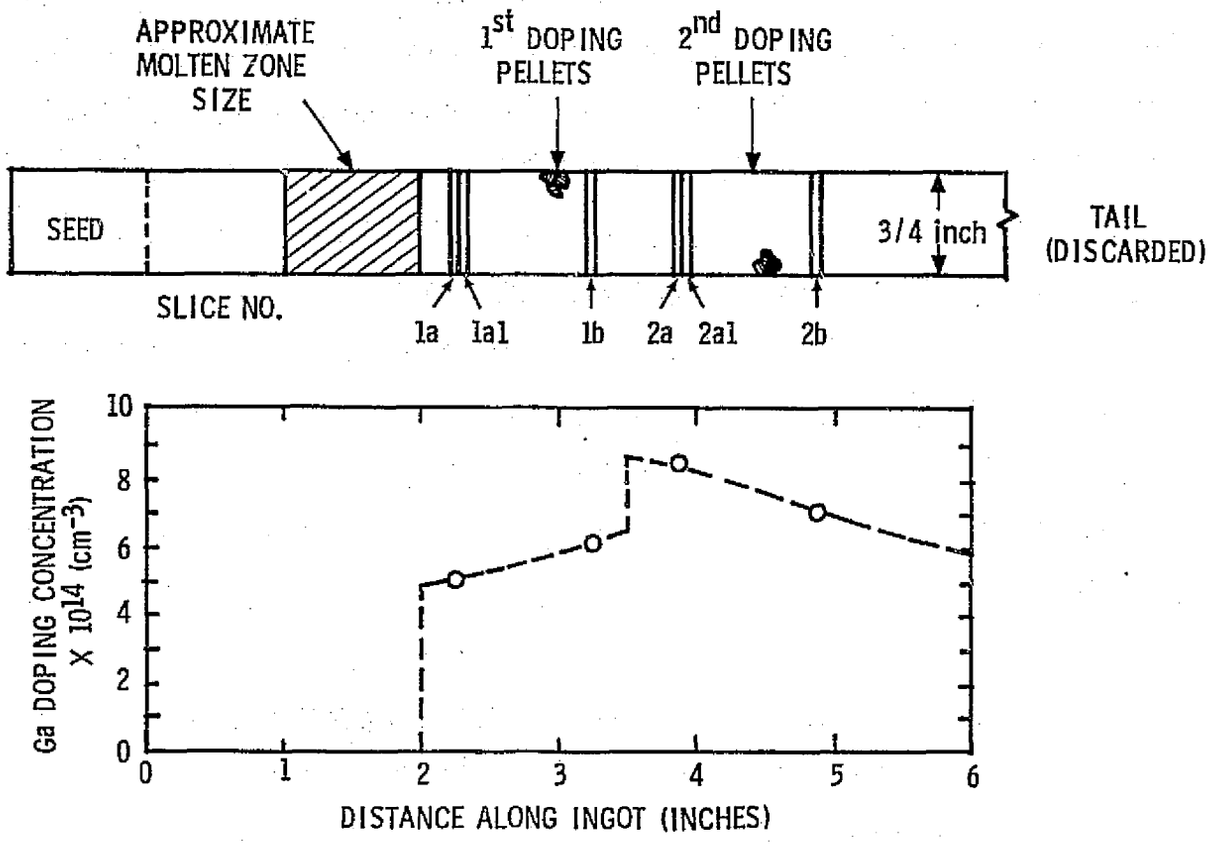

Figure 3-1. Doping Profile for Ge:Ga Crystal No. 5

were given in a previous report[4]. Figures 3-2 and 3-3 show experimentally measured Hall coefficient data versus temperature and the theoretical fit which was obtained for the two samples which were evaluated.

Donor atom concentrations deduced from the comparison between theoretical and experimental data are listed in Table 3-1 for both samples. The residual donor atom concentration in this crystal is in the 10^{10} to 10^{11}/ cm^3 range as was the previous Ge:Ga crystal grown by this same technique. The desired Ga doping concentrations were also obtained. This result demonstrates the reproducibility of the Ge:Ga crystal growth method.

4. Ibid.

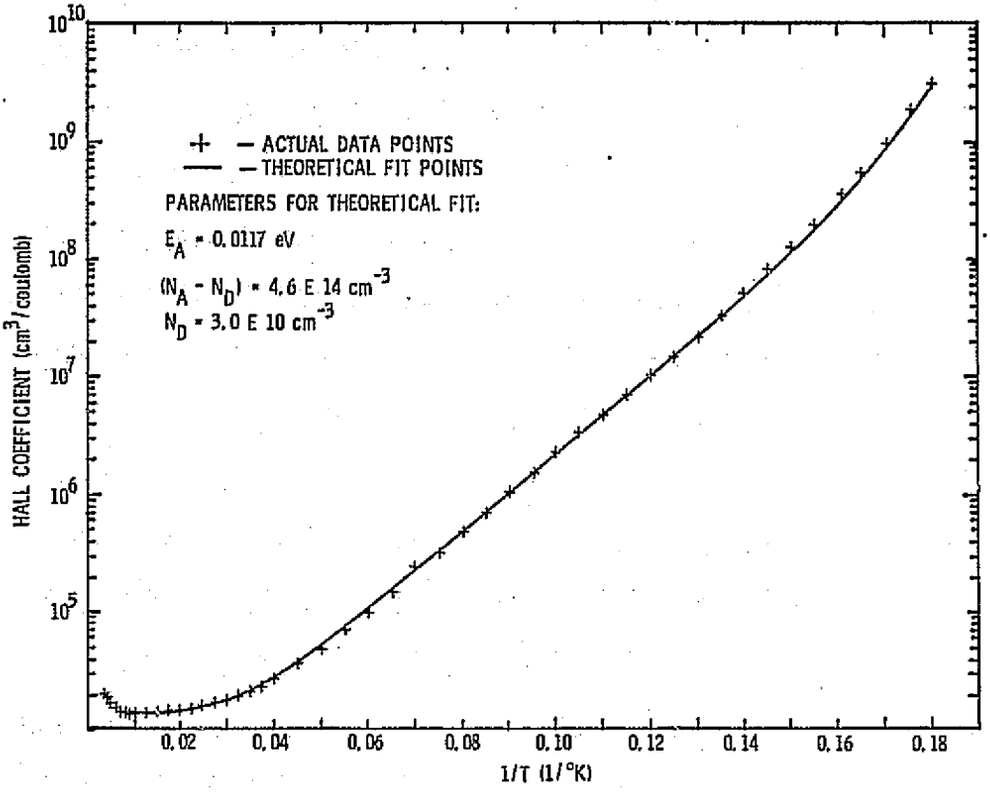

Figure 3-2. Hall Coefficient Versus Reciprocal Temperature for Ge:Ga Sample 5-1a

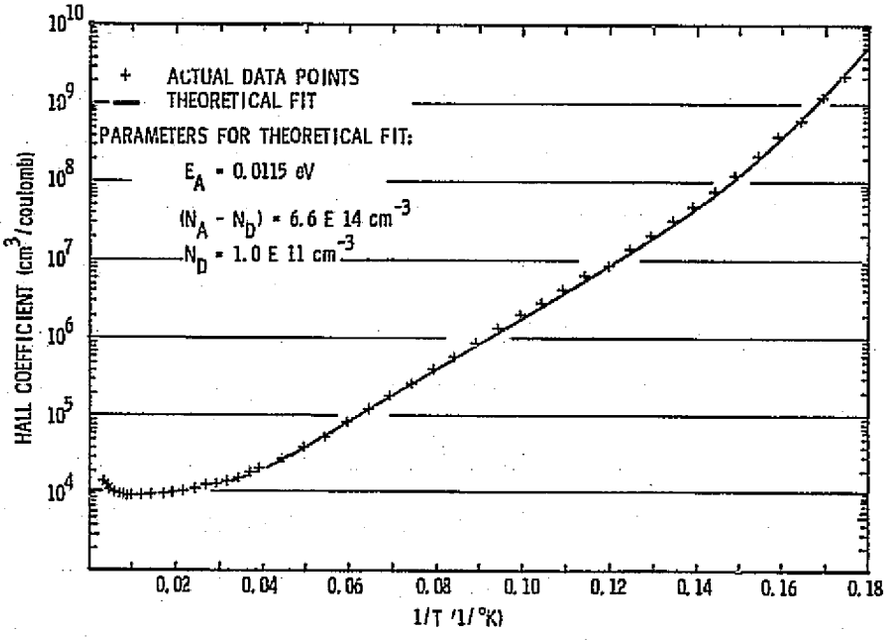

Figure 3-3. Hall Coefficient Versus Reciprocal Temperature for Ge:Ga Sample 5-2a

Table 3-1. Summary of Doping Parameters for Ge:Ga Crystal No. 5

Sample No.	$N_A - N_D$ (cm^{-3})	N_A (cm^{-3})	N_D (cm^{-3})	ϵ_i (eV)
	X 10^{14}	X 10^{14}	X 10^{10}	
Ge:Ga 5-1a	4.6	4.6	3.0	0.0117
5-2a	6.6	6.6	10.0	0.0115

HALL MOBILITY

The Hall mobility is plotted versus temperature in Figure 3-4 for the two samples cut from crystal Ge:Ga 5. At higher temperatures, the mobility is limited by lattice scattering, and both samples have essentially the same mobility. At the lowest temperatures (below 10°K) there is evidence of neutral impurity scattering. In this case, the mobility varies inversely as the concentration of neutral scattering centers, i.e., gallium atoms. From Table 3-1, Sample No. 5-2a is seen to be a factor 1.43 more heavily doped than Sample No. 5-1a. Therefore, the mobility of this sample should be 1/1.43 or 0.70 of No. 5-1a. The experimentally measured ratio is 1.5/2.1 = 0.71, in good agreement with theoretical expectations.

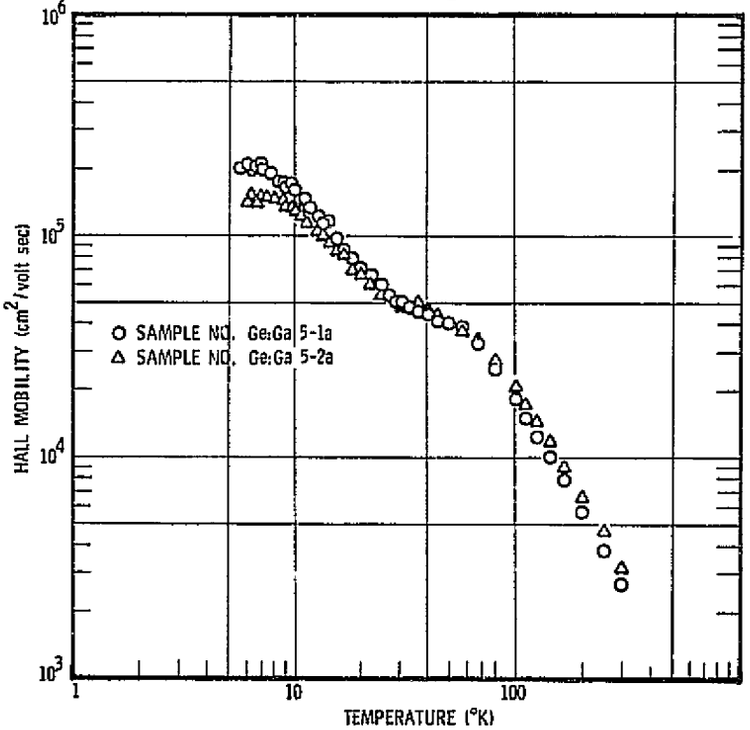

Figure 3-4. Hall Mobility Versus Absolute Temperature for Two Samples from Crystal Ge:Ga 5

RESISTANCE VERSUS TEMPERATURE

Because of equipment limitations, the variable temperature Hall effect measurements do not extend below 5°K. To obtain data at temperatures less than 5°K, a Ge:Ga detector element was obtained and its resistance measured versus temperature over the range from 10° to 3°K. The main objective of this measurement was to determine if impurity hopping conductivity was present. Figure 3-5 shows the circuit diagram used for the measurement. Data were taken with a constant voltage of 0.02 volt applied across the sample producing an electric field strength of 0.04 volt/cm. A carbon resistor thermometer mounted close to the detector sample was used for temperature measurement. Background radiation was excluded from the samples during the measurements.

Figure 3-6 shows the results on two samples from crystal Ge:Ga 5. These samples were taken from the same slice as were the detector samples. In fact, they were surplus detector samples and were, therefore, fabricated in the same manner as detector samples. Both samples show an exponentially rising resistance down to about 4°K. The ionization energies obtained from this part of the curves are 0.0106 and 0.0105 eV in reasonable agreement with the values obtained from the Hall coefficient data. Below 4°K the resistance curves level off at a value of about 10^{10} ohms. The interpretation of this result is that it is due to impurity hopping conductivity. The observation of a resistance plateau at about 10^{10} ohms is in agreement with the measurements made by Fritzsche and Cuevas.[5] However, it would be expected that the sample with higher Ga concentration should exhibit the lower resistance when impurity hopping is present. The data in Figure 3-6 shows the opposite behavior. The reason for this is unknown.

---

5. H. Fritzsche and M. Cuevas, Phys. Rev. 119, 1238 (1960)

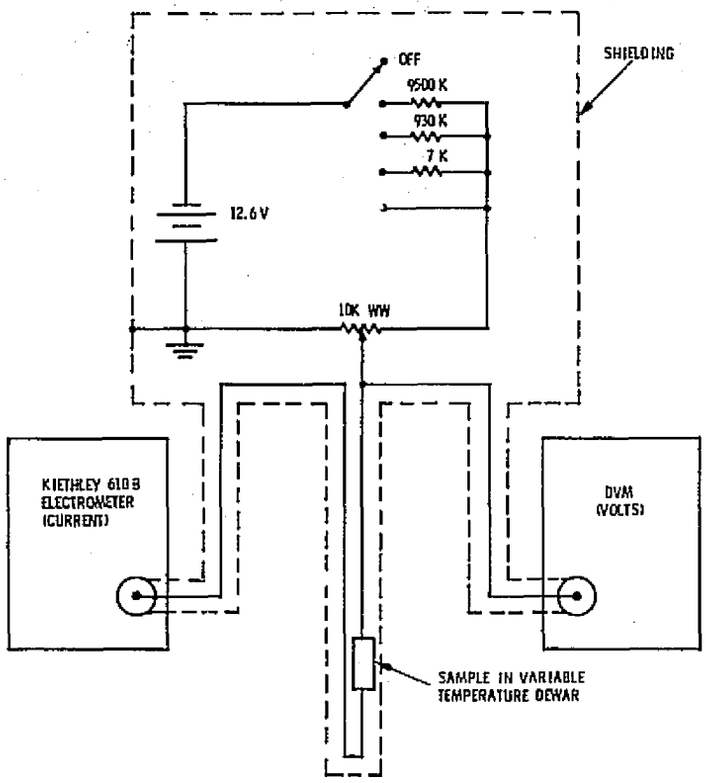

Figure 3-5. Circuit Used for Resistance Versus Temperature Measurements on Detector Samples

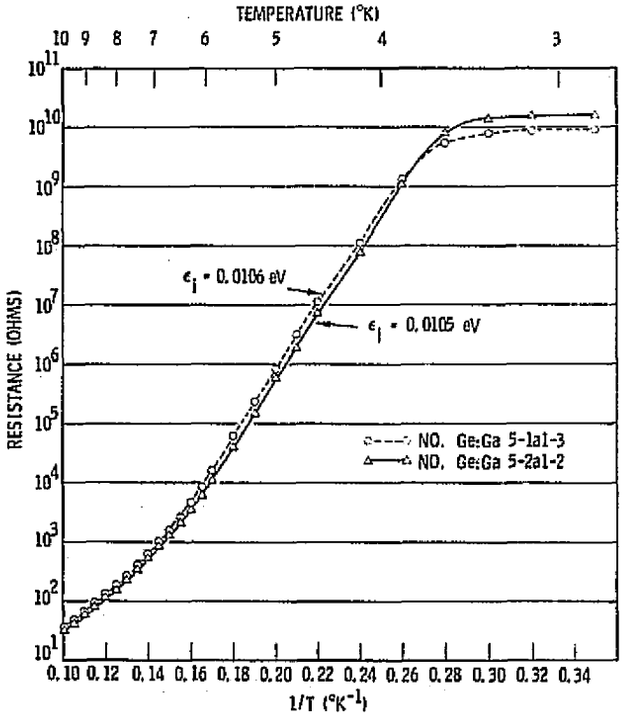

Figure 3-6. Resistance Versus Reciprocal Temperature for Two Ge:Ga Detector Samples from Crystal 5 ($Q_B \approx 0$)

Section 4

Ge:Be CRYSTAL GROWTH AND EVALUATION

Ge:Be CRYSTAL GROWTH

The final report from the work performed under Contract NAS2-9385 [6] discussed in detail the problems encountered in doping the Ge:Be crystals. It had been concluded that most of the Be was going into the crystal, but that it was being made electrically inactive by combining with something, probably oxygen. It was suspected that the hydrogen purifier system that had been used to grow early crystals had a leak that allowed oxygen to enter the furnace. Subsequent crystals (through crystal No. 10) were grown under vacuum, with the objective being to reduce the oxygen content in the melt. This method was considered successful, and, although other problems were encountered while growing crystal No. 10, a Be doping of approximately 1×10^{15} atoms/cm^3 was achieved.

The growth process established for crystal No. 10 was used in the continued development of this program. Crystal No. 11 was grown with the intent of producing two uniform zones within the crystal, doped to 1×10^{15} and 2×10^{15} atoms/cm^3. Evaluation of the crystal, however, showed evidence of an air leak in the vacuum system. One end of the crystal had a Be concentration of 9.1×10^{14} atoms/cm^3. Under normal conditions it would be expected that the dopant level would remain at 9×10^{14} atoms/cm^3 for more than an inch of material. However, the Be concentration dropped to 4.3×10^{13} atoms/cm^3 at a point 1 inch from the measured 9×10^{14} atoms/cm^3. Where the dopant had been added for a Be concentration of 2×10^{15} atoms/cm^3, the measured Be level was only 5.6×10^{13} atoms/cm^3. This is shown graphically in Figure 4-1.

6. P. R. Bratt and N. N. Lewis, op. cit.

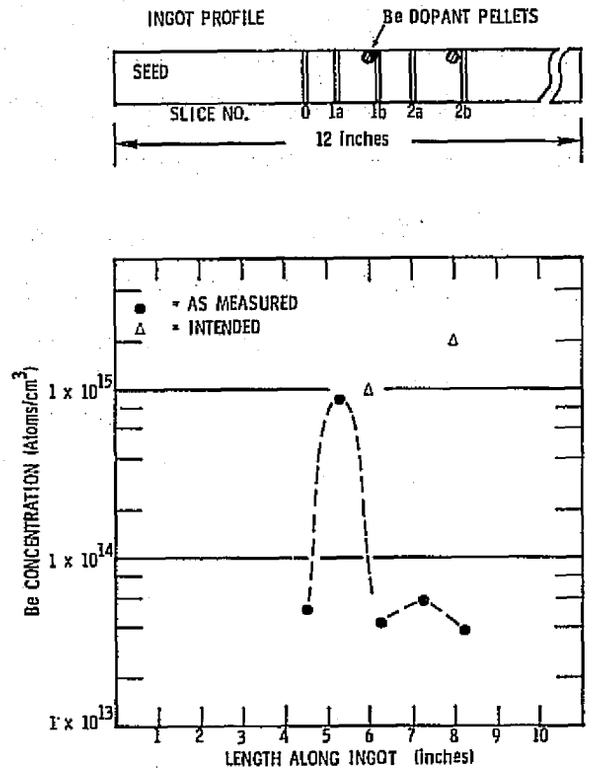

Figure 4-1. Doping Profile for Ge:Be Crystal 11

Steps were taken to repair the portions of the vacuum system that were thought to have contributed to the anomolous results of crystal No. 11, and a second crystal was grown (No. 12), again with the intent to obtain two dopant concentrations. The results of this crystal were similar to No. 11.

While the anomalous results of crystals 11 and 12 were being studied to determine why the Be was not being evenly distributed throughout the crystal, a third crystal (No. 13) was grown. In the interest of time, this was a shorter crystal, and was doped with only one Be level, 2×10^{15} atoms/cm^3. The measured Be concentration was $\simeq 4 \times 10^{15}$ atoms/cm^3 at one end of the crystal, falling off rapidly over the length evaluated.

Growth of crystal No. 14 was begun, after some repairs to the vacuum equipment, but the material and seed were destroyed due to an equipment malfunction.

Crystal No. 15 was then grown, again doping to 1×10^{15} and 2×10^{15} atoms/cm^3. Once again, the desired concentration was achieved at the doping points, but fell off rapidly, as shown in Figure 4-2. This crystal had been compensated with antimony.

After the growth of crystal No. 15, the vacuum equipment was extensively modified, and some refinements of the procedure in growing the crystals were incorporated. The modifications consisted of replacement of the end caps for the quartz tube in which crystals are grown and enlargement of the diameter of the line from the vacuum pump to the quartz tube. In addition to these changes, several passes over the quartz tube were made at elevated temperature (1000°C) before placing the ingot in the tube. After the ingot was placed in the tube, four additional passes were made at a reduced temperature (800°C) to further clean and outgas the tube without melting the ingot.

After this equipment modification, Ge:Be crystal No. 16 was grown. Figure 4-3 shows the results of evaluation of Ge:Be crystal No. 16. From these results it appears that the oxygen source had been eliminated, or at least reduced to an insignificant level. The amounts of Be measured are nearly twice the concentration intended, indicating that more Be per unit added had actually entered the crystal than had been seen in prior attempts.

The vacuum pump used on the system was then replaced with a larger capacity/pumping speed pump, and all O-ring seals were replaced with ball joints. The results of these and the prior modifications to the system can be seen in the results of crystal No. 17, Figure 4-4. The crystal is uniform within the doping regions, and the actual amount of Be in the ingot is near the intended amount. These data indicate that the vacuum problem (allowing the combination of oxygen with Be had been solved, and that better control over the amount of dopant to add for a given Be concentration had been achieved. Crystal No. 17 had also been partially compensated with antimony.

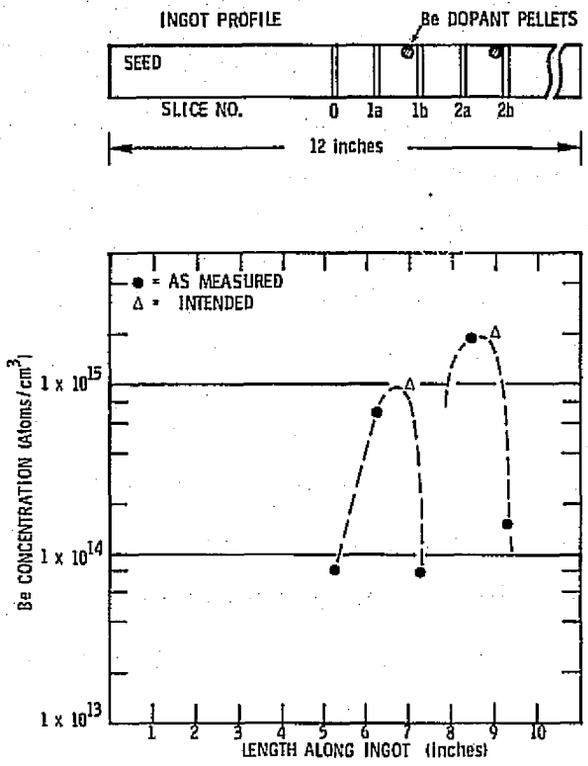

Figure 4-2. Doping Profile for Ge:Be Crystal 15

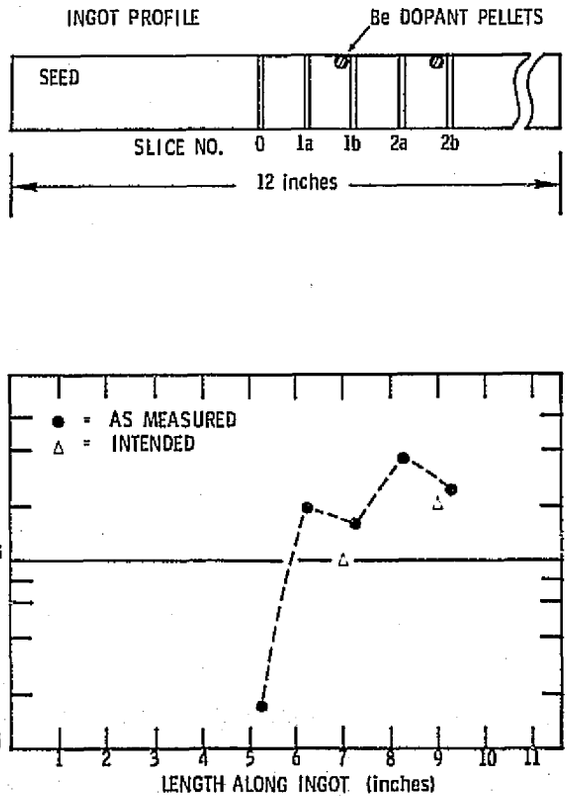

Figure 4-3. Doping Profile for Ge:Be Crystal 16

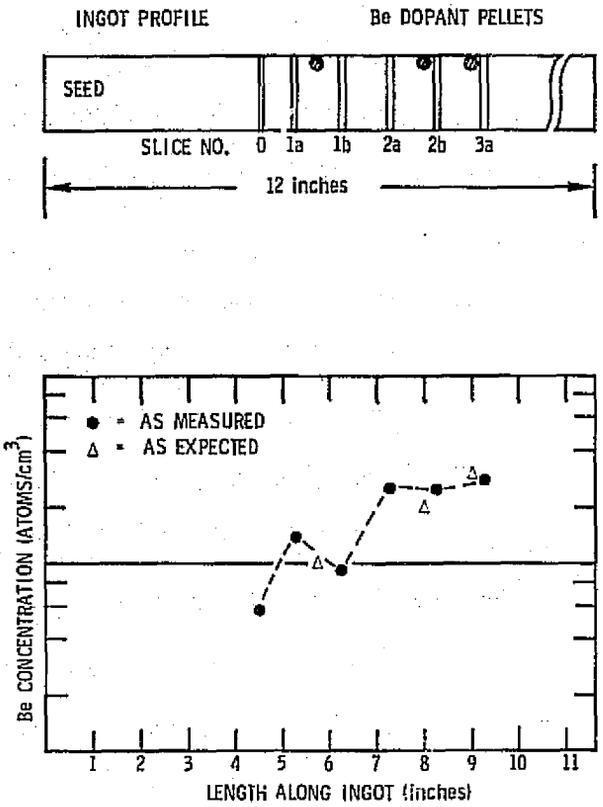

Figure 4-4. Doping Profile for Ge:Be Crystal 17

With these successful results, crystal No. 18 was grown. The intent with No. 18 was to grow a crystal with uniform Be concentration over several inches. Dopant pellets were placed every half-inch along the crystal. After the dopant was added, two passes, one toward the seed and then back again, were made over the crystal. The crystal was uncompensated with intended Be concentration of 2. $\times 10^{15}$ atoms/cm^3.

The results of the evaluation of crystal 18 are shown in Figure 4-5. The crystal is very uniform. The Be concentration is less than intended; however, this can be accounted for by the fact that there was a delay of approximately 15 hours between the first and second passes over the ingot after the dopant was added. During that interval, the zone remained molten and some of the Be diffused out of the ingot.

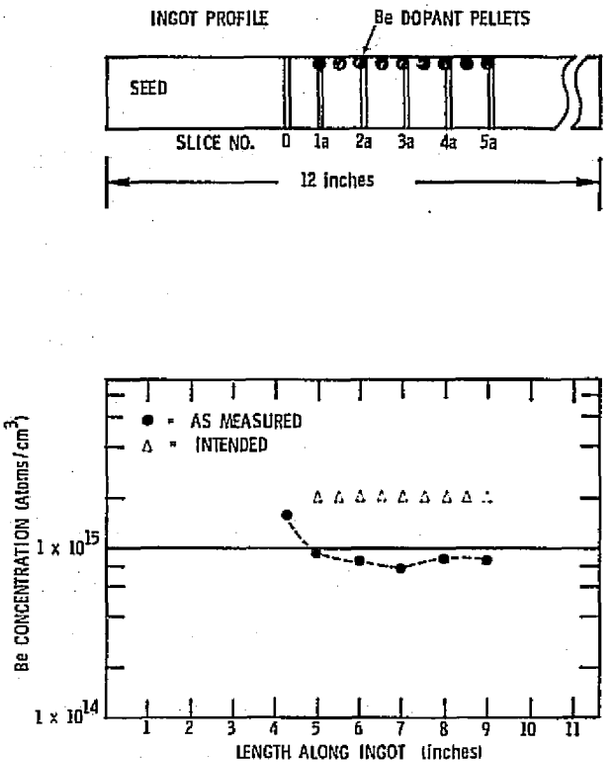

Figure 4-5. Doping Profile for Ge:Be Crystal 18

Since the results from Crystal 18 showed that the technique for doping a crystal to a predetermined amount and obtaining a uniformly doped crystal had been established, it had been intended to grow at least one additional crystal, this time with a higher amount of compensation than previous crystals. The development effort of this program was discontinued, however, before that could be accomplished.

COMPENSATED Ge:Be

After extensive zone refining of Ge, some residual impurities still remain which produce shallow donor and acceptor levels within the Ge band gap. The acceptor levels usually dominate the donors causing the material to be p-type. These shallow acceptors are probably due to B and Al impurities, and their concentration is on the order of 10^{12} to 10^{13} atoms/cm^3. The residual donor concentration is on the order of 10^{10} to 10^{11} atoms/cm^3. The addition of Be to such material produces what we have

called an "uncompensated" Ge:Be crystal. The energy level diagram for such material is shown in Figure 4-6(A). This diagram illustrates the fact that the shallow acceptor atoms are both thermally and optically active at low temperatures. Free holes may be thermally activated out of these centers. Thus, the low-temperature Hall coefficient and resistance versus temperature curves reflect the shallow acceptor levels rather than the deeper Be levels. Optical excitation of free holes from these levels may also occur producing a long-wavelength response beyond the cutoff of the response due to the first Be level. Moore [7] has measured this long-wavelength response and found it to be significant compared to the response from the Be atoms. Thus, for many sensor applications, a long-wavelength cutoff filter would be required to eliminate this long-wavelength response.

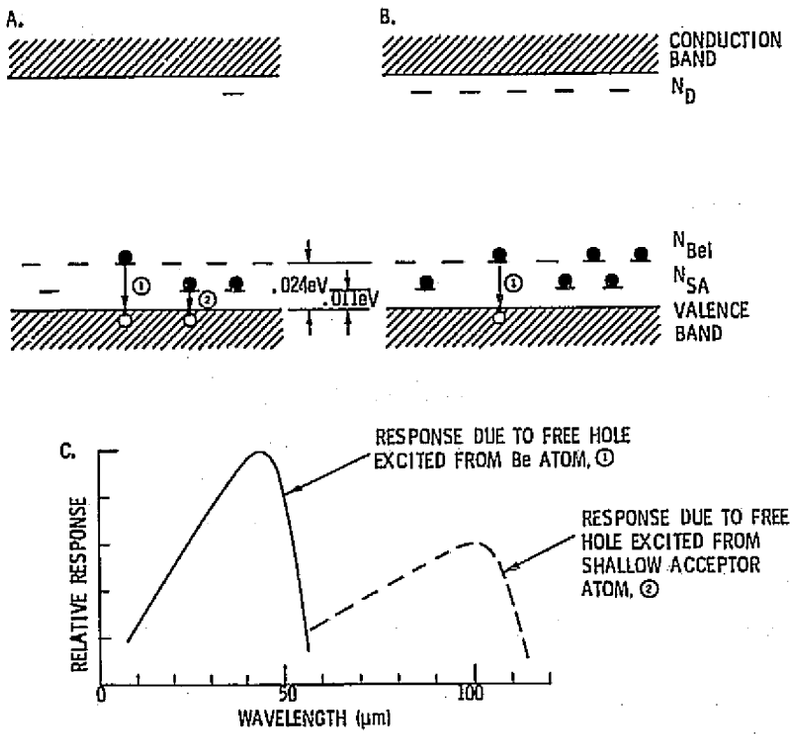

Figure 4-6. A. Energy Band Diagram for Uncompensated Ge:Be
B. Energy Band Diagram for Compensated Ge:Be
C. Relative Spectral Response for Ge:Be Showing Long Wavelength Response Due to Uncompensated Shallow Acceptors

7. W. J. Moore, private communication.

Another way to eliminate this unwanted long-wavelength response is to produce "compensated" Ge:Be material. By this we mean material to which small amounts of donor impurity atoms are added at the same time as the Be dopant. The concentration of donor atoms should be just slightly greater than the residual acceptor concentration. Then at low temperatures, electrons from the compensating donor will fill all of the residual shallow acceptors as well as some of the Be levels. This situation is shown in Figure 4-6(B). Now the shallow acceptors are effectively inactive as to their influence on the thermal and optical activation of free holes. However, they may possibly take part in the free hole recombination process either as trapping or recombination centers.

In the production of compensated Ge:Be material, one attempt to make the added donor concentration just slightly greater than the residual acceptor concentration. This keeps the number of compensated Be atoms to a minimum. If too many donors are added and the number of electrons residing on Be levels becomes too large, the free hole lifetime will be seriously degraded. This, in turn, can degrade the detector responsivity. During this contract phase, three Ge:Be crystals were grown which were intentionally compensated with Sb donor atoms. These were Ge:Be crystal Nos. 15, 16 and 17. The Hall data analysis of the next section present the results of this effort.

Ge:Be CRYSTAL EVALUATION

Preliminary evaluation of Ge:Be crystals was made by Hall effect measurements at room temperature. Since the Be atom is a double acceptor in Ge with ionization energies of 0.024 and 0.064 eV, each Be atom will contribute two free holes at room temperature. Thus the hole concentration calculated from the measured Hall coefficient must be divided by two to obtain the concentration of electrically active Be centers. A magnetic field strength of 15 kgauss was used in the room temperature Hall measurements. Examples of some of the results of these measurements were given in the previous section.

Selected Ge:Be samples were subjected to Hall effect measurements versus temperature. Analysis of these data provides additional information on the crystal doping parameters such as concentration of shallow acceptor impurities (probably B or Al) and compensating donor impurities. A four-level model was used to analyze the Ge:Be variable temperature Hall data. These levels are: one shallow acceptor, one shallow donor, and the two Be levels. Based on this model, theoretical Hall coefficient curves were generated and fit to the experimental data by adjusting the values of the various dopant concentrations. Further details of this analysis were presented in the previous report.[8]

Figure 4-7 shows Hall coefficient versus temperature data taken on sampler from crystals Ge:Be 11 and Ge:Be 15. The solid line represents the theoretical fit to the data points which are shown as crosses. Table 4-1 gives the activation energies and doping concentrations used to generate the theoretical curves. It is to be noted that these two crystals have about the same Be concentration. However, crystal 15 was intentionally compensated with a small amount of S6 donors whereas crystal 11 was not. This has the effect of raising the magnitude of the Hall coefficient curve in the low-temperature range and in clearly demonstrated in the Figure. The intent was to totally compensate all the shallow acceptor levels by making N_D just slightly larger than N_{SA}. If this is done, the Hall coefficient curve will take on a shape shown by the dotted line in Figure 4-7. The data in Table 4-1 as well as the Figure show that this attempt failed by only a narrow margin.

Figure 4-8 shows Hall coefficient data on two other samples that were tested from crystals 16 and 17. These crystals had about twice the amount of Sb compensation added as for crystal 15. However, it was still insufficient to totally compensate the shallow acceptors, undoubtably due to the fact that these crystals contained more shallow acceptors than crystal 15.

---

8. P. R. Bratt, op. cit.

Figure 4-7. Hall Coefficient Versus Reciprocal Temperature for Ge:Be Samples 11-1a-2 and 15-2a-2

Figure 4-1. Doping Parameters Obtained from Theoretical Fit of Four-Level Model to Ge:Be Hall Samples

PARAMETER	UNITS	SAMPLE NUMBER	
		11-1A-2	15-2A-2
(Be_1)	eV	0.0218	0.0219
(Be_2)	eV	0.0710	0.0737
(SA)	eV	0.0132	0.0100
N(Be)	cm^{-3}	1.25×10^{15}	1.60×10^{15}
N(SA)	cm^{-3}	1.64×10^{13}	3.39×10^{12}
N(D)	cm^{-3}	4.56×10^{10}	2.38×10^{12}

ϵ = IONIZATION ENERGY IN eV
N = DOPING CONCENTRATION IN cm^{-3}
Be_1 = FIRST Be ACCEPTOR LEVEL
Be_2 = SECOND Be ACCEPTOR LEVEL
SA = SHALLOW ACCEPTORS
D = SHALLOW DONORS

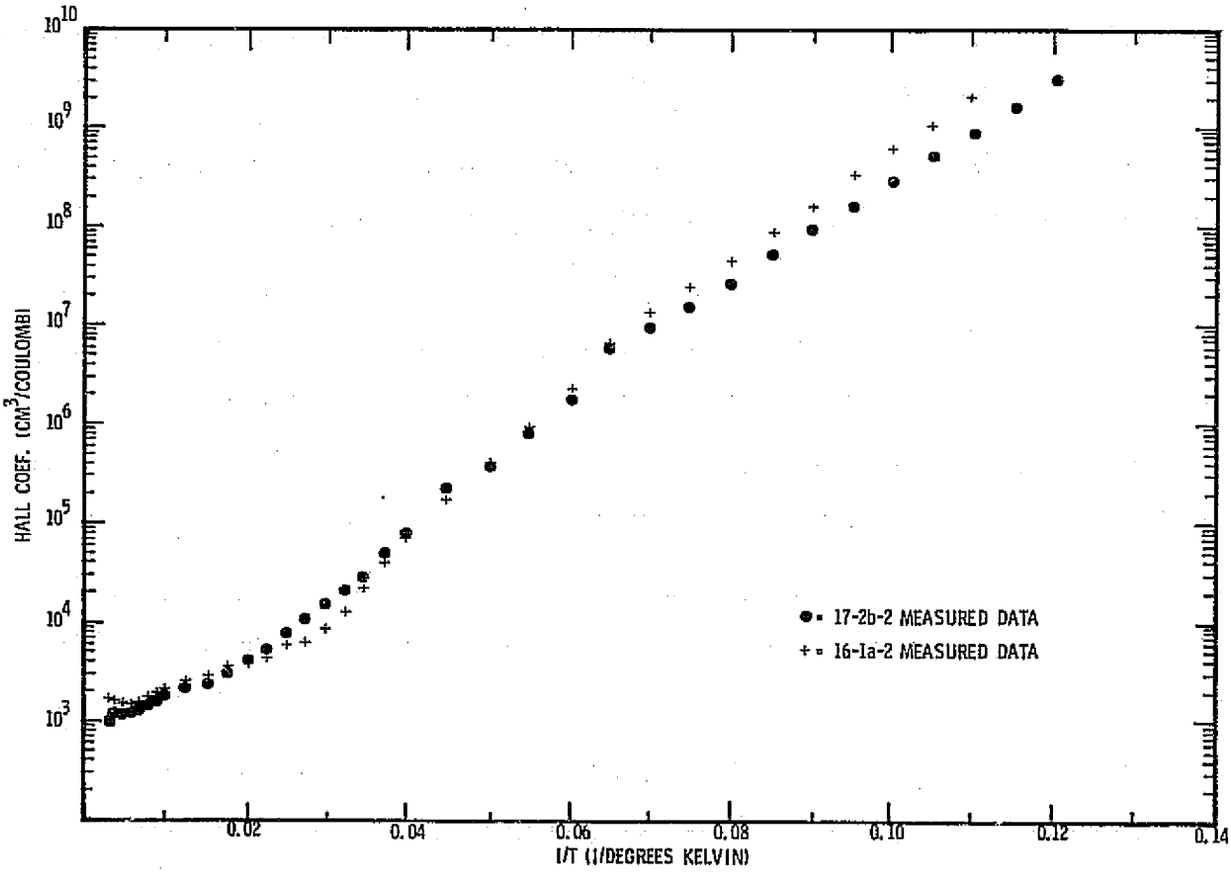

Figure 4-8. Hall Coefficient Versus Reciprocal Temperature for Ge:Be Samples 16-1a-2 and 17-2b-2

Close compensation is a delicate art in crystal growth as evidenced by this work. One attempt to keep the Sb concentration low enough to just slightly over-compensate the shallow donors. This must be done because excessive amounts of compensation result in decreases in the free hole lifetime which could be detrimental to detector responsivity. Because of the early termination of the program, work on compensated Ge:Be crystal growth could not be completed. Enough information was obtained, however, to be able to proceed in future crystal runs with confidence that proper compensation can be achieved.

HALL MOBILITY

The Hall mobility measured on three Ge:Be samples is shown in Figure 4-9 as a function of temperature. All samples show a continually rising mobility down to the lowest temperature attained. The more heavily doped sample, Ge:Be 17-2B-2 exhibits a somewhat lower mobility in the low-temperature range presumably due to neutral impurity scattering.

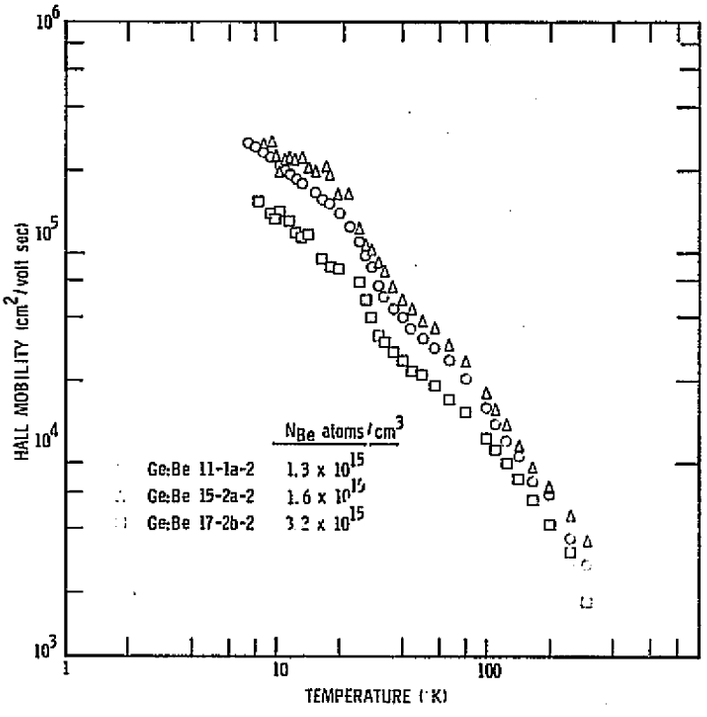

Figure 4-9. Hall Mobility Versus Temperature for Ge:Be Samples

Section 5

DETECTOR FABRICATION AND TEST

DETECTOR FABRICATION

Detector chips were cut from the Ge:Ga or Ge:Be crystals and fabricated into detector elements using standard processing technology which was previously developed at SBRC. Electrical contacts to the detector were formed by ion implantation of boron ions. This produces a p^+-p contact with uniform p^+ doping and a highly planar interface with the p-type crystal bulk. Each detector element was assembled onto a tungsten metal mount along with a load resistor and cryogenic preamplifier. This assembly is shown in Figure 5-1. The load resistor had a nominal value of 5×10^{10} ohms at 3°K. The MOSFET was a Hughes W164 p-channel enhancement mode device.

All Ge:Ga detectors fabricated during this phase of the work were cut from two slices of crystal Ge:Ga 5, 1a1 and 2a1, with Ga doping concentrations of 4.6×10^{14} and 6.6×10^{14} atoms/cm^3. Figure 3-1 shows the location of these slices in the ingot. The Ge:Be detectors were fabricated from several of the crystals produced, with Be concentrations ranging from 9.1×10^{14} to 2.5×10^{15} atoms/cm^3.

LOW BACKGROUND TEST DEWARS

The detector assemblies were mounted to a two-part copper heat sink which was designed to provide a vise-like clamping of the tungsten detector mount to the copper heat sink. This design was chosen to obtain good thermal conduction to the detector mount. A carbon resistor thermometer was imbedded in a hole drilled into the copper heat sink. Figure 5-2 shows a sketch of the heat sink design.

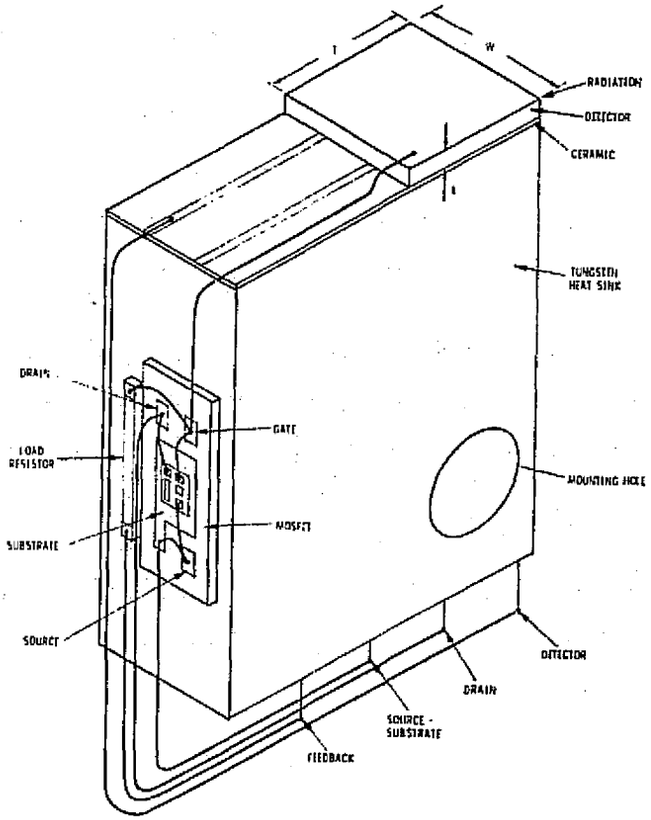

Figure 5-1. Detector — Cryogenic Preamplifier Assembly

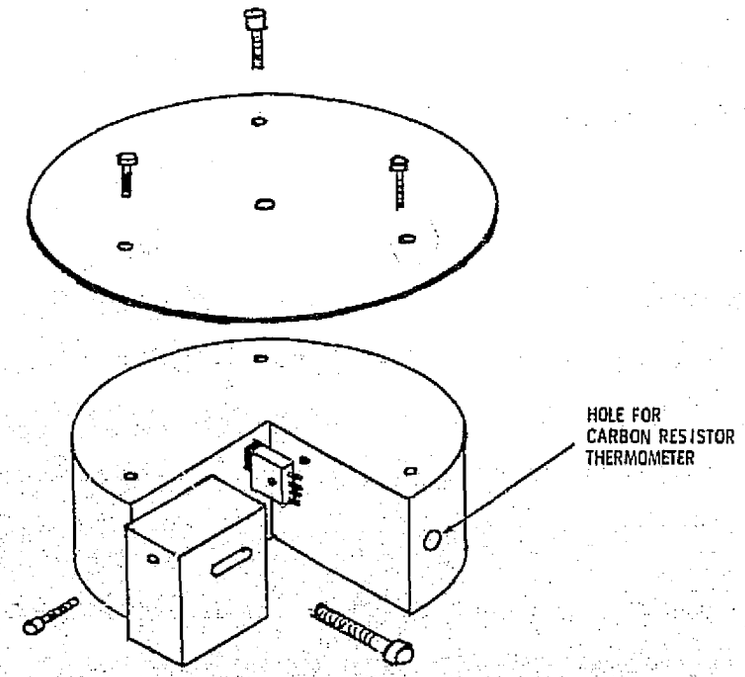

Figure 5-2. Sketch of Copper Heat Sink for Mounting Detector-Preamplifier Assemblies to the Low-Background Test Dewar

This copper heat sink was mounted in a Janis Model RD liquid helium dewar. An aperture defining the sensitive area ($\frac{1}{2}$ mm x $1\frac{1}{2}$ mm for Ge:Be; 1 mm x $1\frac{1}{2}$ mm for Ge:Ga) of the detector was placed directly over the detector and a baffle plate with 2.0 mm diameter aperture was placed directly over that. This configuration was used in an effort to prevent stray radiation from getting to the sides of the detector. A series of aperture plates and cold filters were located between the detector and the dewar outer window to provide the desired attenuation of background radiation. Figures 5-3 and 5-4 show the filtering arrangements used in testing Ge:Ga and Ge:Be detectors.

The background photon flux density arriving at the detector plane was calculated from the following formula.

$$Q_B(\Delta\lambda) = Q(300^\circ K, \Delta\lambda)\, T_R \sin^2\theta/2 \qquad (3)$$

where $Q(300^\circ K, \Delta\lambda)$ = photon irradiance from 2π sterradians of $300^\circ K$ blackbody radiation integrated over the filter pass-band.

T_R = total peak transmittance of all filters.

θ = detector field-of-view angle defined by aperture and distance from detector to aperture.

The details of this calculation for the different low-background conditions used in detector evaluation are presented in Appendix A.

For Ge:Ga, the cold filtering consisted of two special black polyethylene filters and two neutral density filters. The special black polyethylene* acts as a long-pass filter with a cut-on wavelength of about 80 μm. It is a scattering filter made by mixing various alkali halide crystal powders together with polyethylene and hot rolling them into a thin film. Some carbon particles also may be in the mixture. The true constituents in the film are not known

*We are grateful to K. Shivanandan of NRL for supplying us with this filter material and its relative spectral transmittance curve.

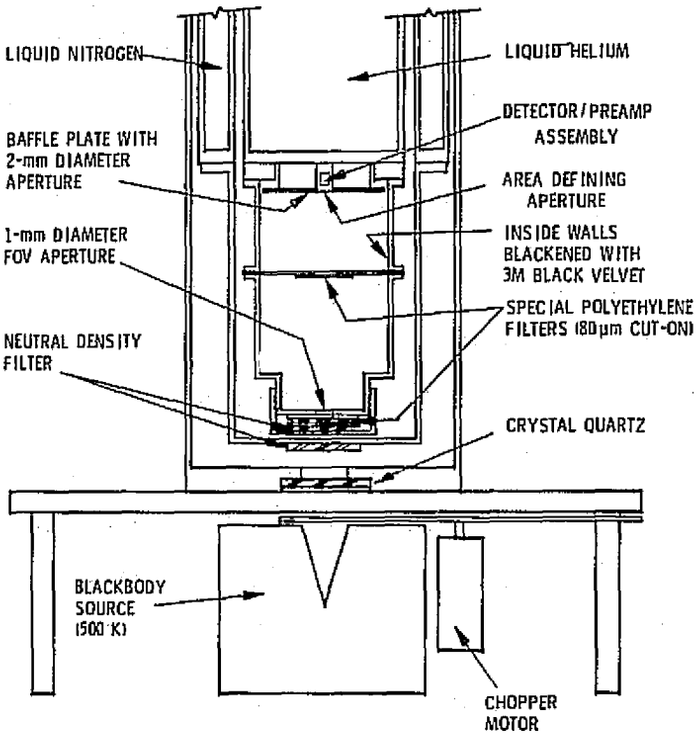

Figure 5-3. Low-Temperature, Low-Background Dewar Setup for Testing of Ge:Ga Detectors at 100 μm

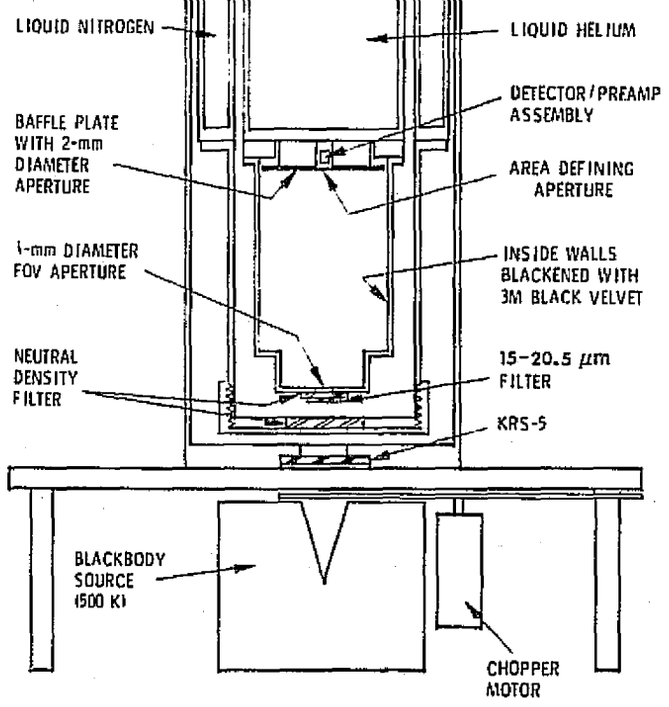

Figure 5-4. Low-Temperature, Low-Background Dewar Setup for Testing of Ge:Be Detectors

to us. The neutral density filters were made at SBRC by evaporating a thin-nichrome metal film onto z-cut crystal quartz flats. The relative spectral transmittance of these filters was not measured, but was assumed to be essentially flat in the 60- to 120-μm range. The average transmittance of these filters was checked at room temperature by placing each filter in front of a dewar containing a Ge:Ga detector (also filtered to detect only radiation beyond about 60 μm) and measuring the attenuation of the detector signal from the 500°K blackbody source.

In all the Ge:Ga detector testing done on this program, a filter combination was used which gave a calculated background flux $Q_B = 3.7 \times 10^8$ photons/cm^2/sec at the detector plane.

For Ge:Be detector testing, a combination of a 15- to 20.5 μm multilayer interference band-pass filter* and two neutral density filters was used. In this case, the neutral density filters were made by evaporating nichrome metal onto germanium flats. This filtering combination had worked well for testing doped Si detectors in past work at SBRC and was easy to implement for the Ge:Be detectors. Due to the unavailability of the bandpass filter for most of the program period for the Ge:Be tests, some of the detector testing was performed without a bandpass filter, in the interest of time. Background flux levels for these tests must be considered as best estimates. In other tests, a 25-μm cut-on filter was used to test in the 30- to 50-μm range. Extrapolation of NEP data from the 15- to 20.5-μm range to 50 μm can be made with little additional expected error. The filter combination used for Ge:Be detector testing gave a calculated background photon flux at the detector of $Q_B = 1.2 \times 10^9$ photons/cm^2 sec. Table 5-1 shows the filtering combinations used for the various detectors, and the estimate of the background flux levels.

* Obtained from Optical Coating Laboratories, Inc.

Table 5-1. Filtering Combinations Used for Ge:Be Testing

Detectors Tested	Window	Neutral Density Filters (Ge)	Other Filters	Q_B ph/sec/cm^2
11-1a1-1	Ge	1.5% and 1.6%	None	$\approx 6 \times 10^9$
15-2a1-1	KRS-5	1.5% and 1.6%	None	$\approx 1 \times 10^{10}$
16-1a1-1	KRS-5	1.5% and 1.6%	25 μm cut-on*	$\approx 6 \times 10^8$
17-1a1-1	KRS-5	1.5% and 1.6%	25 μm cut-on*	$\approx 6 \times 10^8$
17-2b1-1	KRS-5	1.5% and 1.6%	15 - 20.5 μm	1.2×10^9

*Sapphire with ZnO, diamond scattering and poly AR coating (Infrared Laboratories Inc., Tucson, Arizona)

The signal radiation was obtained from a 500°K blackbody located in close proximity to the dewar outer window. A variable speed chopped provided modulation frequencies from 1 to 1000 Hz. The blackbody has a large opening and the detector "looks into" this opening through the small FOV defining aperture located within the dewar. Therefore, the blackbody radiation is effectively emanating from this aperture rather than from the blackbody cavity itself. The blackbody signal irradiance at the detector plane is given by the formula

$$H_{BB}(\Delta\lambda) = \frac{W_{BB}(\Delta\lambda)\, A_{BB}\, T'_R F}{\pi D^2} \qquad (4)$$

where $W_{BB}(\Delta\lambda)$ = blackbody radiant emittance integrated over filter passband

A_{BB} = FOV defining aperture area

T'_R = total filter transmittance

F = chopper form factor

D = aperture to detector distance

The signal irradiance on the detector is due to the temperature difference between the 500°K blackbody cavity and the room temperature chopper blade (assumed to be at 300°K). Therefore the signal photon flux density impinging on the detector is greater than the 300°K background photon flux density. For noise measurements, the blackbody opening is covered with a shutter so that the detector then only sees 300°K background photons.

The blackbody radiant emittance was numerically integrated over the filter pass-band to obtain that fraction $W_{BB}(\Delta\lambda)$ which would pass through the filter. The details of this calculation are given in Appendix A.

The chopper wave-form factor is used to convert peak-to-peak signal irradiance values to root-mean-square values. For the chopper used, this factor had a value of 0.40. A listing of all the parameter values used in Equations (5) and (6) are given in Table 5-2.

Table 5-2. List of Parameters Used in Blackbody Irradiance Calculations

Parameter	Units	Ge:Ga	Ge:Be
$W_{BB}(\Delta\lambda)$	w/cm^2	3.29×10^{-4}	1.62×10^{-2}
A_{BB}	cm^2	7.85×10^{-3}	7.85×10^{-3}
T'_R		3.85×10^{-5}	1.47×10^{-4}
T_R		6.1×10^{-5}	2.4×10^{-4}
D	cm	9.58	8.59
F		0.40	0.40
$H_{BB}(\Delta\lambda)$	$w(rms)/cm^2$	1.38×10^{-13}	3.22×10^{-11}
θ	degrees	0.60	0.60
$Q_B(300°, \Delta\lambda)$	photons/sec cm^2	1.49×10^{17}	5.68×10^{17}
$Q_B(\Delta\lambda)$	photons/sec cm^2	2.5×10^{8}	4.6×10^{9}

TEST PROCEDURE

All testing was done in a screen room. Tests were performed using a source follower cryogenic preamplifier and the external circuit components shown in Figure 5-5. The preamplifier output was coupled to a Quan Tech Model 206C amplifier which provided a voltage gain of 10^3. Amplifier frequency response was flat between 1 Hz and 100 kHz. The low-frequency gain was -3 db at 0.5 Hz. Signal and noise readings were taken on a Quan-Tech Model 304 Wave Analyzer and also visually monitored on an oscilloscope.

Tests were designed with the object of evaluating detector performance as a function of frequency, voltage, and temperature. Not all dependencies were studied on all detectors, in the interest of time, however. Temperatures below 4.2°K were obtained by pumping over the liquid helium reservoir of the Janie Dewar. A calibrated carbon resistance thermometer mounted in a hold drilled into the copper heat sink shown in Figure 5-2 was used to monitor detector temperature.

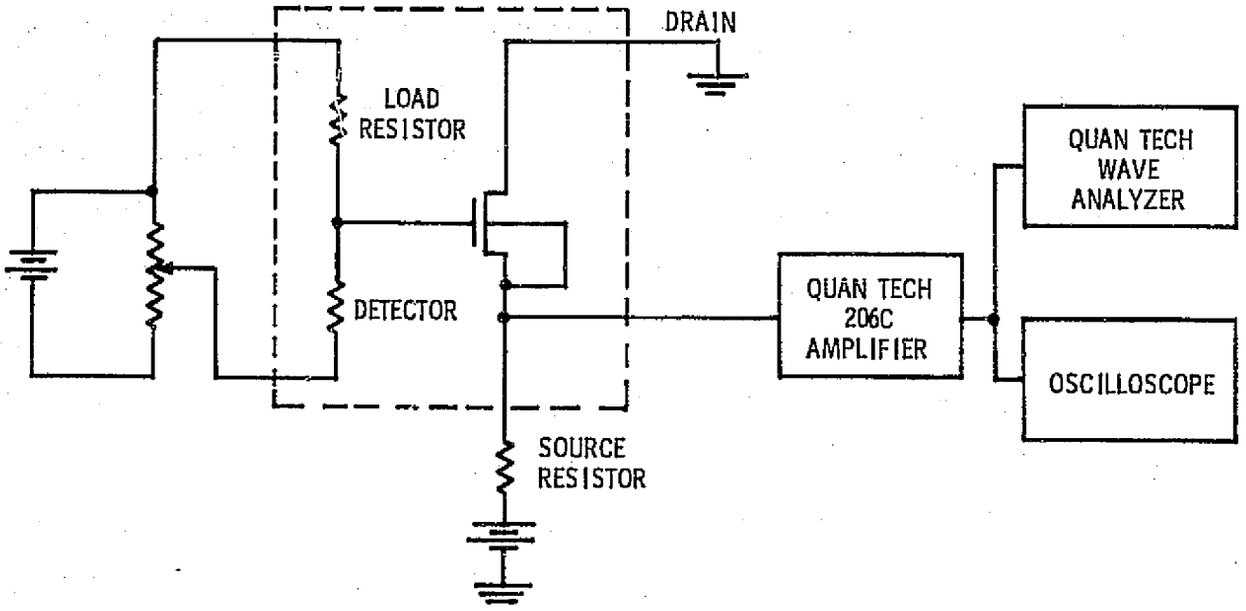

Figure 5-5. Diagram of Circuit Used for Ge:Ga and Ge:Be Detector Tests

Note: Circuit elements within dashed line are at cold temperature, those outside are at room temperature.

RESULTS — Ge:Ga DETECTORS

Three Ge:Ga detectors were tested, one from slice 5-2a1, and two from slice 5-1a1. No signals were obtained on either of the 5-1a1 detectors. No tests were made to determine if this was a result of material problems, detector processing problems, or test setup problems. It was determined, however, that the resistances of both detectors were 4 to 8 x 10^9 Ω, an order of magnitude lower than resistances of the detectors made from crystal No. 4 on the previous contract.

The detector from slice 5-2a1 (5-2a1-1) showed optimum S/N ratio when operated at a bias voltage of 0.059 volt. The NEP values for this detector ranged from 2 to 4 x 10^{-16} watt, in the frequency range from 1 Hz to 800 Hz, at 2.5 °K, and with a background flux of 3.7 x 10^{8} photons/sec/cm^2. This is a factor of 2 to 3 times higher than would be expected at this background, based on the results of the No. 4 crystal.

Detailed data from this detector are plotted in Figures 5-6, 5-7 and 5-8. The data were taken at 2.5°K; we were unable to achieve 2.0°K during the first test, and since the NEP was high and the resistance low, the test was discontinued.

Figure 5-6 shows that the detector resistance decreases with increased bias. This is due primarily to an increase in free carrier density because of an increasing lifetime with bias. Signal and noise voltages increase at a rate somewhat greater than linearly with bias. This may also be due to an increasing free carrier lifetime. There is no evidence of signal saturation in this detector as might be expected if the sweep-out limit were being approached.

The detector signal data in Figure 5-7 can be used to calculate detector responsivity values and from these one can obtain estimates of quantum efficiency and photoconductive gain. The voltage responsivity at wavelength λ is a function of frequency due to the circuit RC rolloff. This frequency dependence can be written as

$$R_v(\lambda, f) = R_v(\lambda, o)\,[1 + (2\pi f \tau_{RC})^2]^{-\frac{1}{2}} \qquad (5)$$

where $R_v(\lambda, o)$ is the dc or low-frequency responsivity and τ_{RC} is the circuit response time. By fitting a curve having the functional dependence on frequency shown by this equation to the signal data in Figure 5-7 it was found that the 1-Hz responsivity values are sufficiently close to the

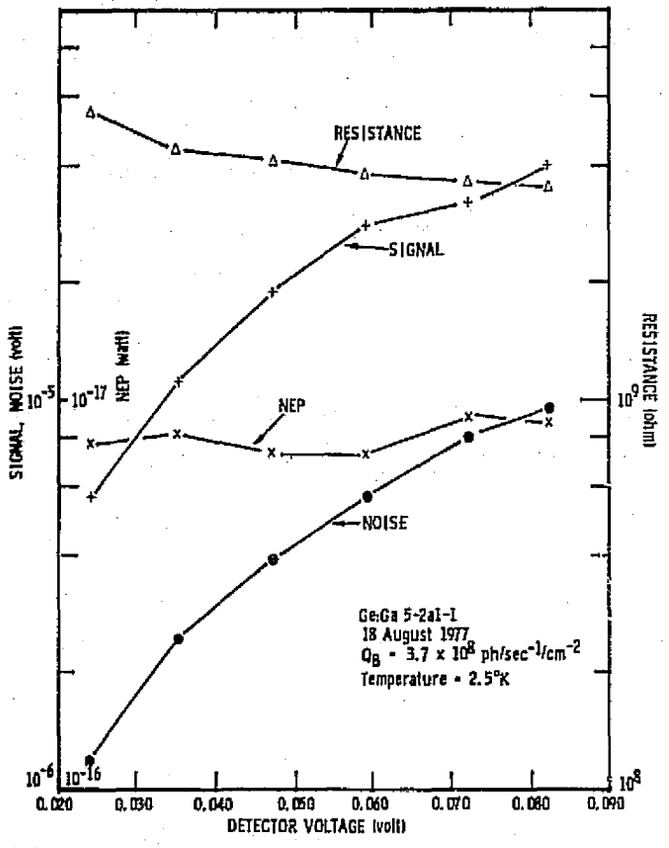

Figure 5-6. Signal, Noise, NEP and DC Resistance Versus Bias Voltage for Ge:Ga Detector No. 5-2a1-1 at 2.5°K

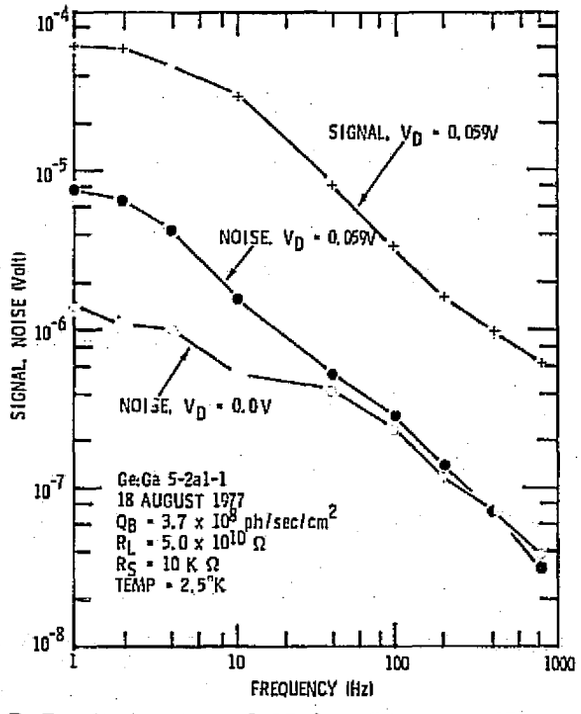

Figure 5-7. Signal and Noise Versus Frequency for Ge:Ga Detector 5-2a1-1 at 2.5°K

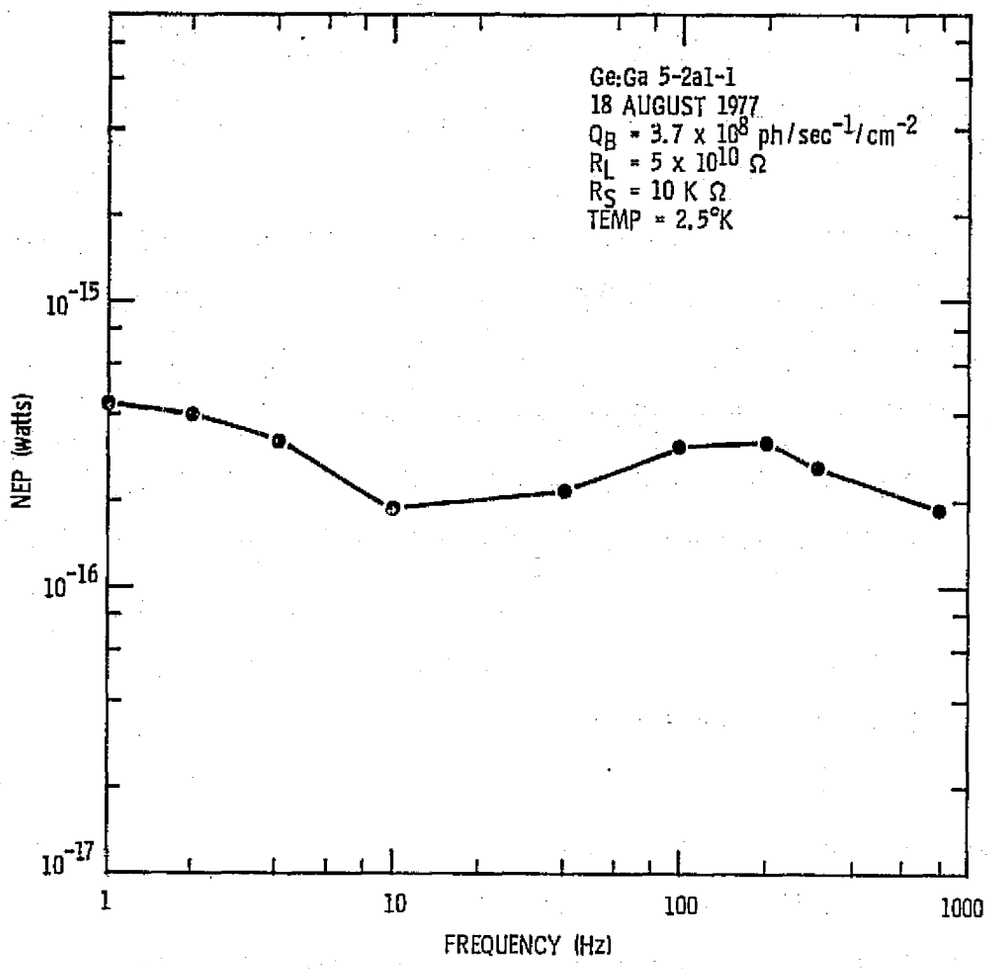

Figure 5-8. NEP Versus Frequency for Ge:Ga Detector 5-2a1-1 at 2.5°K

dc value to be used in an approximate calculation. The 1-Hz voltage responsivity was calculated from experimentally measured data using the formula

$$R_v(\lambda, 1) = \frac{S(\Delta\lambda)}{H_{BB}(\Delta\lambda)A_D g} \qquad (6)$$

where $S(\Delta\lambda)$ = signal voltage measured at output of preamplifier

$H_{BB}(\Delta\lambda)$ = blackbody irradiance at detector (see Table 5-1)

A_D = detector area (1.5×10^{-2} cm^2)

g = preamplifier gain (0.85).

The short-circuit current responsivity was calculated from the voltage responsivity using the equation

$$I_s(\lambda, 1) = R_v(\lambda, 1)/R_{||} \tag{7}$$

where $R_{||}$ is the parallel resistance formed by the load and the detector ac resistance values,

$$R_{||} = \frac{R_{ac}R_L}{R_{ac} + R_L}, \tag{8}$$

and

$$R_{ac} = R_{dc}\left[1 - \frac{V}{R_{dc}}\frac{dR_{dc}}{dV}\right]^{-1}. \tag{9}$$

According to detector theory, the short-circuit current responsivity is given by

$$I(\lambda, o) = \frac{\eta e \lambda}{hc} G_{pc} \tag{10}$$

where $G_{pc} = \frac{\tau \mu E}{L}$ = photoconductive gain

τ = free-hole lifetime

μ = hole mobility

E = electric field strength

L = interelectrode spacing

η = quantum efficiency

e = electronic charge

λ = wavelength

h = Planck's constant

c = speed of light.

Therefore, once a value for $I(\lambda, o)$ is obtained, some estimates of values for η and G_{pc} can be made.

Using the foregoing equations and the measured experimental data, the value of current responsivity was calculated for the Ge:Ga detector to be 6.37 A/W at 2.5°K. The current responsivity value is at the peak of the detector's spectral response curve which was taken to be 100 μm. This value of current responsivity is comparable to that obtained in previous

Ge:Ga crystals and is considered to be quite good for a detector which is not mounted in an integration chamber. It implies an ηG_{pc} product of 0.08. Therefore, if η were 0.3, G_{pc} would be 0.27 which is below the sweep-out limited value of 0.5.

The measured signal-and-noise data were used to calculate the NEP data which are shown in Figure 5-8. The NEP versus frequency data shows an essentially flat behavior with a small decrease as the frequency increases.

As stated previously, no further testing (i.e., NEP versus temperature, NEP versus background flux level) was performed on this detector because of its marginal performance.

RESULTS — Ge:Be DETECTORS

Detectors were fabricated and tested from Ge:Be crystal 11, 15, 16, and 17 on this program. Crystals 12 and 13 were not processed beyond the Hall data samples since the doping level of No. 12 was nearly identical to that of No. 11, and the Hall data from No. 13 showed evidence of too high a Be concentration. Detector studies from crystal No. 18 were not completed before the development effort was discontinued.

Crystals 15, 16, and 17 were partially compensated with antimony, although test results showed the compensation level to be less than desired. Crystals 11, 12, 13, and 18 were grown from uncompensated material.

Because of the filtering limitations in testing the Ge:Be detectors, detector 17-2b1-1 is the only detector for which quantitative analysis is accurate. Figures 5-9 through 5-11 illustrate the relationship between bias voltage, resistance, signal noise, and NEP for this and other detectors.

Figure 5-9 shows the measured signal and noise data versus frequency at 3°K for several detectors. The signal data for only one of these detectors was analyzed in the same way as for the Ge:Ga detectors to obtain short-circuit current responsivity values and estimates of the ηG_{pc} product. The results are given in Table 5-2. The blackbody signal radiation was restricted

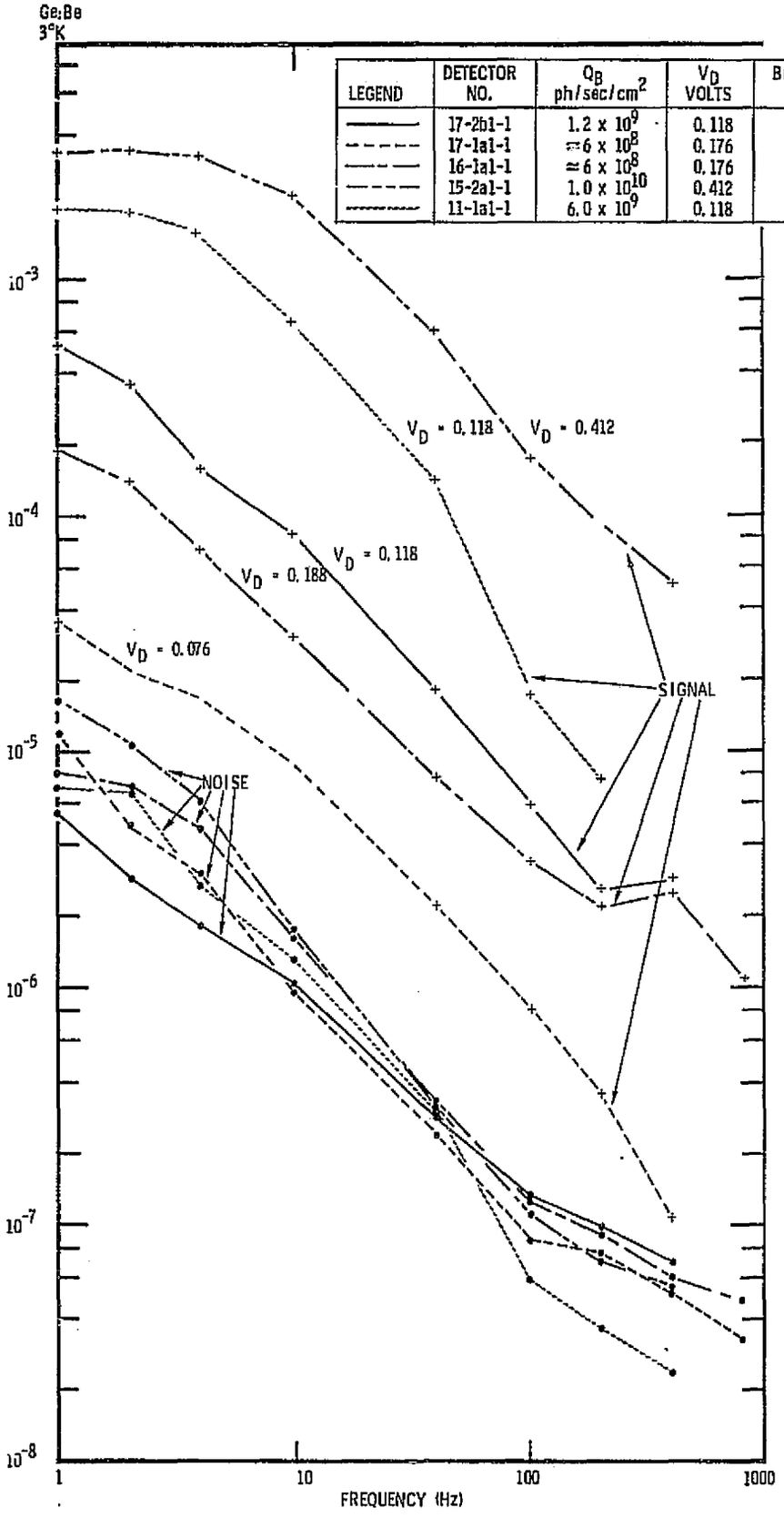

Figure 5-9. Signal and Noise Versus Frequency for Ge:Be Detectors at 3.0°K

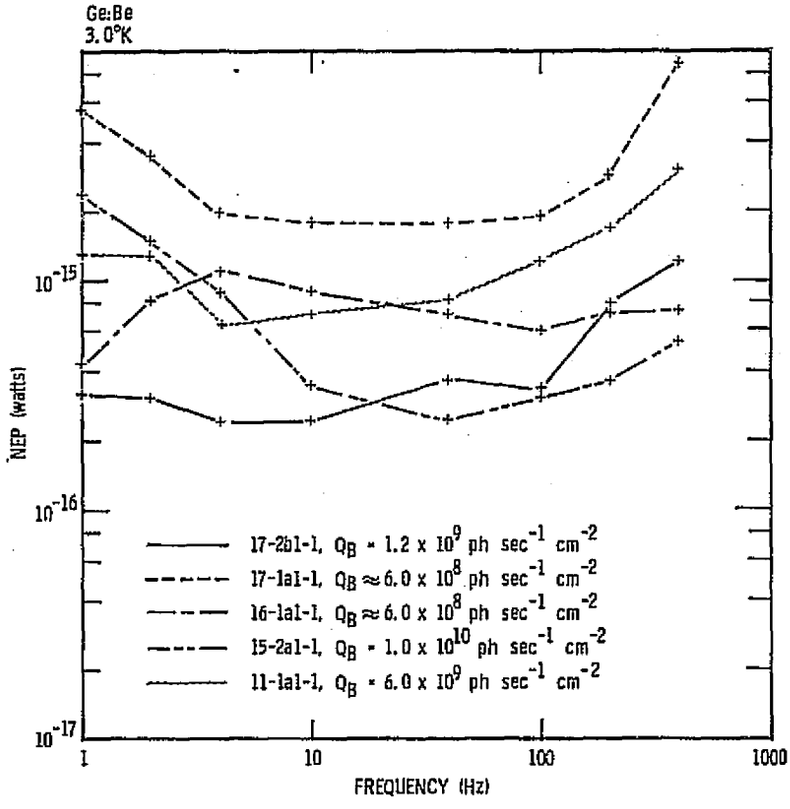

Figure 5-10. NEP Versus Frequency for Ge:Be Detectors at 3.0°K

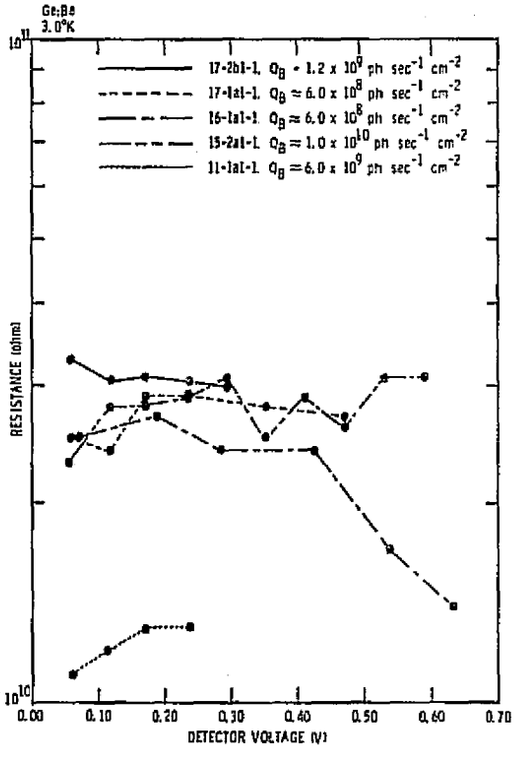

Figure 5-11. DC Resistance Versus Detector Voltage for Ge:Be Detectors at 3°K

Table 5-2. Parameters Used in Calculation of Short-Circuit Current Responsivity for Ge:Be Detector 17-2b1-1

PARAMETER	UNITS	DATA	TEMPERATURE (°K)
BIAS VOLTAGE	VOLTS	0.118	3.0
ELECTRIC FIELD	VOLTS/CM	2.36	3.0
R_{ac}	OHMS	2.6×10^{10}	3.0
$S(\Delta\lambda, 1)$	MILLIVOLTS	0.99	3.0
$R_V(\lambda p, 1)$	VOLTS/WATT	4.2×10^{10}	3.0
$I_s(\lambda p, 1)$	AMPS/WATT	2.6	3.0
ηG_{pc}		0.08	3.0

$R_L = 5 \times 10^{10}$ OHMS (NOMINAL VALUE)

$\lambda_p = 40\ \mu m$

$A_D = 7.5 \times 10^{-3}\ cm^2$ (1.5 x 0.5 mm)

$f = 1$ Hz

to the 15- to 20.5-μm band by a filter. Therefore, direct use of Equation (6) gives the voltage responsivity at a wavelength of about 19 μm. To convert this value to responsivity at the peak of the Ge:Be spectral response which is at 40 μm, the calculated responsivity was multiplied by a factor of 2. This factor is based on the relative spectral response of Ge:Be reported by Shenker, et al.[9] The values of voltage and current responsivity listed in Table 5-2 are at the detectors peak wavelength of 40 μm. The calculated current responsivity is 2.6 amp/watt. If one assumes a quantum efficiency of 0.3, then the photoconductive gain would be 0.27. This is a reasonable value for the low-frequency gain (1 Hz) which would not be limited by carrier sweep-out.

Calculated NEP values at 3.0°K are plotted versus frequency in Figure 5-10. Figure 5-10 shows the NEP of 17-2b1-1 to be essentially flat with

9. H. Shenker, E. M. Swiggard and W. J. Moore, Trans. Metallurgical Soc. of AIME, 239, 347 (1967)

frequency between 1 and 10 Hz, and then rising for higher frequencies. Detectors 17-1a1-1, 15-2a1-1, and 11-1a1-1 appear to have some excess noise in the 1- to 2-Hz range causing an increased NEP at these low frequencies.

Figure 5-11 shows detector dc resistance at 3.0°K as a function of detector voltage. The resistance of 17-2b1-1, 17-1a1-1, and 15-2a1-1 appears relatively flat with bias voltage. The resistance of detector 11-1a1-1 is 2 to 3 times lower than other detectors, although the background flux was midrange. The low resistance could be a result of background leaks in the test dewar or the lack of compensation in the crystal material. The resistance of 16-1a1-1 is relatively flat at low voltages, but falls off sharply with an electric field of $\gtrsim$ 8 V/cm. (applied voltage of 0.40 volt).

NEP (10 Hz) and resistance versus temperature for detector 17-2b1-1 are shown in Figure 5-12. The NEP data point at 3°K is probably erroneously high, and should be down between 2 and 3 x 10^{-16} watt/Hz$^{\frac{1}{2}}$. Another measurement at this temperature (see Figure 5-10) showed such an NEP value. The NEP values achieved by this detector are comparable to what was obtained on the previous contract with Ge:Be crystal No. 10. This demonstrates that the addition of compensating donor atoms does not degrade detector NEP in the 2° to 3°K range.

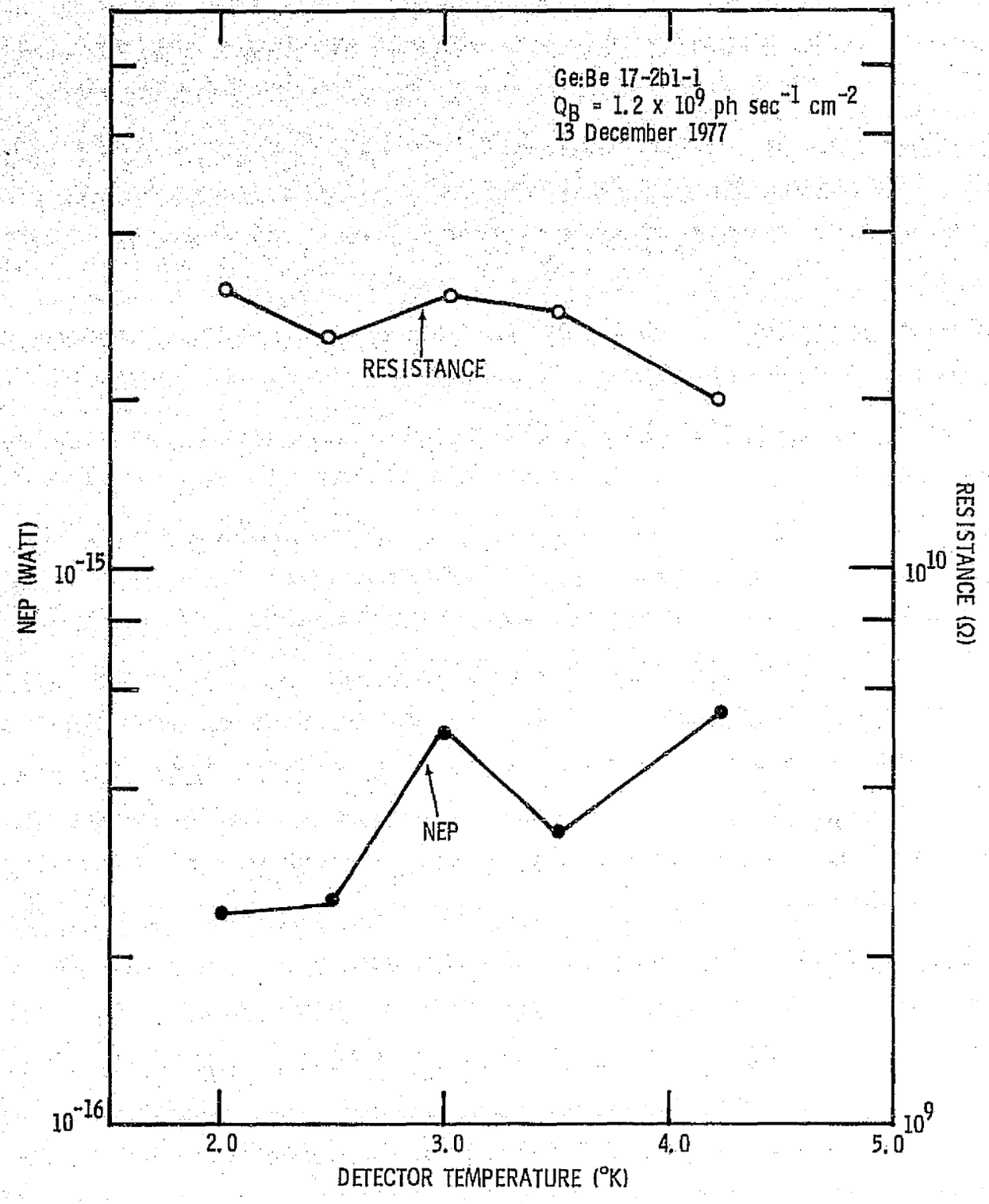

Figure 5-12. NEP and dc Resistance Versus Detector Temperature

Section 6
CONCLUSIONS

The work described in this report has provided significant advances especially in the technology of Ge:Be and, when reviewed in conjunction with the previous work, in the technology of Ge:Ga photoconductors for use in astronomical observations at wavelengths from 30 to 120 Um. The primary conclusions that can be drawn from the work performed thus far are as follows.

Ge:Ga DETECTORS

From previous work:

- A Ge purification method was developed which reduces the residual donor impurity concentration to the 10^{10} atoms/cm^3 range. Residual acceptor impurity content may be much higher but is inconsequential to detector performance.
- Introduction of Ga by the zone leveling method was shown to produce uniformly doped ingots with sufficient material for fabrication of many detectors. The doping concentration can be controlled within an acceptable tolerance.
- Short-circuit current responsivity for 100 μm radiation has been measured to be in the range of 6 to 10 amps/watt at 3.0° K operation. This implies an ηG_{pc} product of 0.074 - 0.124. Quantum efficiency was estimated to be around 0.25.
- Detectors were not enclosed in an integrating cavity. The use of such a scheme could significantly improve quantum efficiency.
- An NEP of 4×10^{-17} watts/$Hz^{\frac{1}{2}}$ had been measured on a Ge:Ga detector at 1 Hz with a background flux of 3.7×10^8 photons/sec/cm^2 at 3.0°K operating temperature. This compares favorably with the calculated BLIP value of 1.2×10^{-17} watts/$Hz^{\frac{1}{2}}$ ($\eta = 0.30$, $\lambda_p = 100$ Um).
- The NEP is minimized at an operating temperature very close to 3.0°K. Higher or lower operating temperatures may cause a degradation of NEP.

- Reproducibility and yield of good detector elements were excellent for Ge:Ga detectors. Most of the technology development on this material has been completed and the producibility of detectors which meet or exceed the NEP objectives for the IRAS mission has been demonstrated.

From current program:

- Crystals doped to 4.6 and 6.6 x 10^{14} Ga atoms/cm^3 exhibit hopping conductivity at temperatures below 2.5°K. The low background NEP of this material is inferior to that of the crystal grown on the previous program which was doped to 2.5 x 10^{14} Ga atoms/cm^2.

Ge:Be DETECTORS

From previous work:

- Oxygen must be eliminated during growth of Ge:Be crystals to prevent Be-O complexing. A vacuum zone melting process was developed which provided a method for doing this, and improved to the extent of being able to dope the crystals to predetermined levels.

- With uncompensated Ge:Be, the NEP is optimized at 3.0°K or lower. There was no clear indication of a minimum in the NEP versus temperature plot.

- The yield of Ge:Be detectors from a given slice of material is good. There is no reason to believe that the yield of Ge:Be detectors should be any different from that of Ge:Ga detectors, once a good crystal has been grown.

- Detectors were not enclosed in an integrating cavity. The use of such a scheme could significantly improve quantum efficiency.

- The Be concentration should be kept below 2 x 10^{15} atoms/cm^3 to prevent impurity hopping conductivity from seriously lowering detector resistance at 3.0°K.

- The electric field strength that can be applied to uncompensated Ge:Be is limited to less than 10 v/cm due to impact ionization of shallow acceptor levels.

- Short-circuit current responsivity for 40 μm radiation was measured to be in the range of 2 to 5 amps/watt for 3.0°K operation.

From the current program:

- Uniform Be doping over a whole Ge:Be ingot was demonstrated using a zone leveling method.
- The addition of Sb donors to compensate shallow acceptors does not degrade detector performance. Tests were made only on partially compensated material; full compensation was not achieved on this program.
- The lowest measured NEP for Ge:Be detectors was 2 to 3×10^{-16} watts/$Hz^{\frac{1}{2}}$ at a frequency of 1 Hz with a background flux of 1.2×10^{9} photons/sec/cm^2. The BLIP value for this background is 4.6×10^{-17} watts/$Hz^{\frac{1}{2}}$ ($\eta = 0.3$, $\lambda_p = 40$ μm).

Appendix A
IRRADIANCE CALCULATIONS

This appendix presents details of the calculation of blackbody signal irradiance and background photon flux density at the detector focal plane in the low-background test dewars.

Ge:Ga TEST DEWAR

As mentioned in Section 5, in the main text, the Ge:Ga detectors were tested using a long-wavelength pass filter consisting of two pieces of "special" black polyethylene and crystal quartz. These materials, along with the detector's natural cutoff at about 120 μm produced a relative spectral response as shown in Figure A-1.* This isolated a spectral band about 35 μm wide in the 100-μm region. Neutral density filters were also used to further attenuate the background photon flux on the detector.

The effective blackbody signal irradiance on the detector was calculated by numerically integrating the blackbody flux over the filter spectral range. To do this, the spectral range was broken up into intervals each 5 μm wide as shown in Figure A-1. The blackbody radiant emittance for each spectral interval was then obtained from a radiation slide rule. These values are shown in Table A-1 along with the spectral intervals and the relative filter transmittance in each spectral interval. Since the signal radiation is produced by the difference between the 500 K blackbody and a 300°K chopper blade, these values were obtained from the slide rule and one was subtracted from the other to obtain the actual signal radiant emittance in each interval. The difference values are listed in column 5 of the table. Multiplication of each number in column 5 by the corresponding relative filter transmittance

*SBRC is indebted to K. Shivanandan of NRL for furnishing these data.

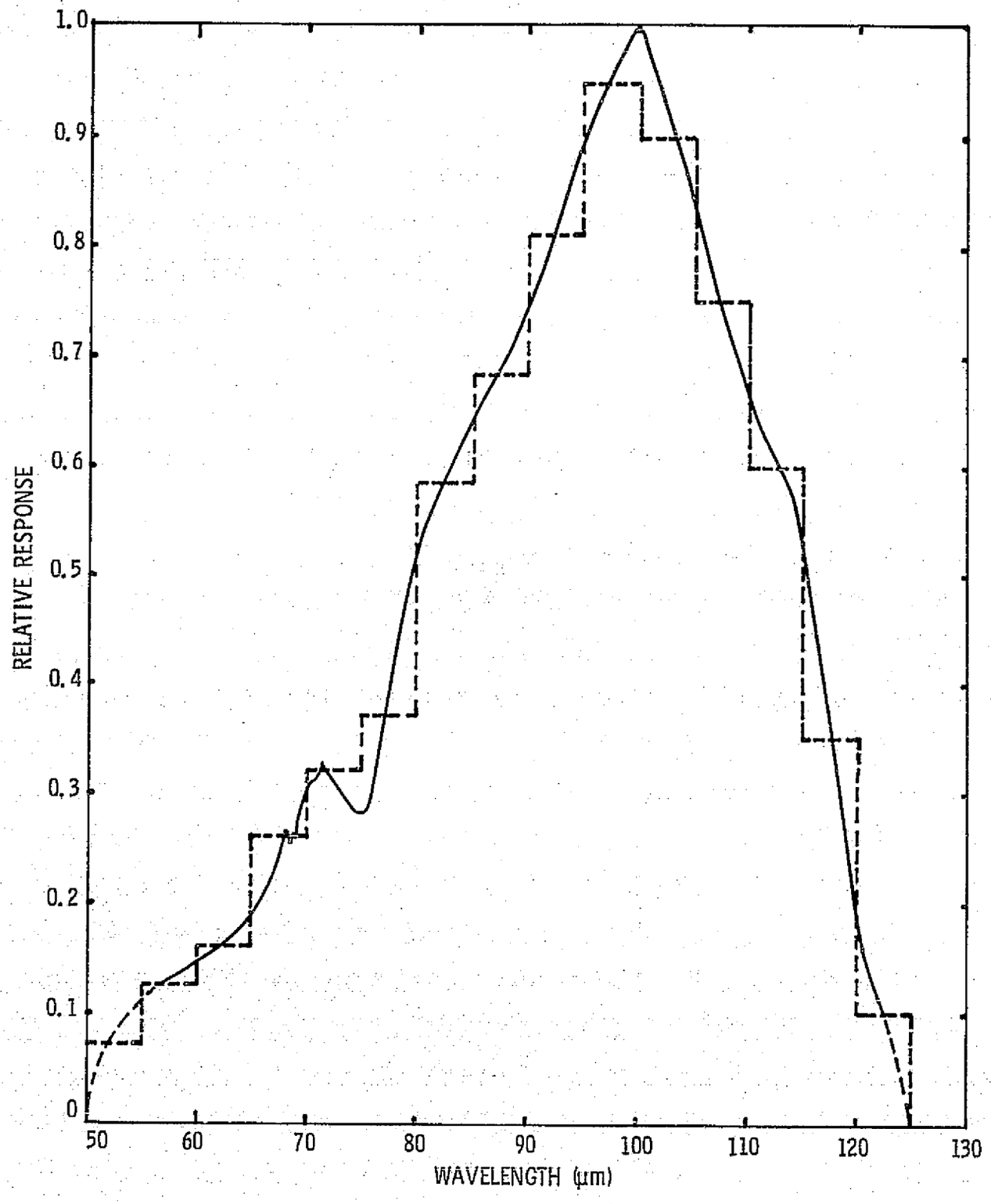

Figure A-1. Relative Spectral Response of Ge:Ga Detector with Long Wavelength Pass Filter

Table A-1. Listing by Spectral Interval of Blackbody Signal Radiant Emittance and Background Photon Flux Values Used for Ge:Ga Detector Testing

(1) λ (μm)	(2) $R_F(\lambda)$	(3) $W_{500}(\lambda)$ (w/cm^2)	(4) $W_{300}(\lambda)$ (w/cm^2)	(5) $W_{500}(\lambda) - W_{300}(\lambda)$ (w/cm^2)	(6) $W_{BB}(\lambda)$ (w/cm^2)	(7) $Q_{300}(\lambda)$ (ph/sec/cm^2)	(8) $Q_B(\lambda)$ (ph/sec/cm^2)
		x 10^{-3}	x 10^{-3}	x 10^{-3}	x 10^{-5}	x 10^{17}	x 10^{16}
40-45	0	1.436	0.670	0.766	0	1.430	0
45-50	0	0.912	0.444	0.468	0	1.060	0
50-55	0.070	0.632	0.310	0.322	2.254	0.818	0.57
55-60	0.125	0.454	0.230	0.224	2.800	0.664	0.83
60-65	0.165	0.334	0.172	0.162	2.673	0.540	0.89
65-70	0.260	0.248	0.130	0.118	3.068	0.441	1.15
70-75	0.320	0.190	0.100	0.090	2.880	0.364	1.17
75-80	0.375	0.150	0.080	0.070	2.625	0.312	1.17
80-85	0.585	0.118	0.062	0.056	3.276	0.257	1.50
85-90	0.685	0.094	0.050	0.044	3.014	0.220	1.51
90-95	0.810	0.076	0.040	0.036	2.916	0.186	1.51
95-100	0.950	0.058	0.032	0.026	2.470	0.157	1.49
100-105	0.900	0.050	0.028	0.022	1.980	0.144	1.30
105-110	0.750	0.040	0.020	0.020	1.500	0.108	0.81
110-115	0.600	0.032	0.018	0.014	0.840	0.102	0.61
115-120	0.350	0.030	0.016	0.014	0.490	0.094	0.33
120-125	0.100	0.027	0.014	0.013	0.130	0.086	0.09
SUMMATION				$W_{BB}(\Delta\lambda) = 3.29 \times 10^{-4}$		$Q_B(300, \Delta\lambda) = 1.49 \times 10^{17}$	

in column 2 gives the effective blackbody radiant emittance in each spectral interval. These values are listed in column 6. Summation overall spectral intervals then gives the total blackbody radiant emittance in the filter pass band.

This total radiant emittance number is then used in Equation (6) to calculate the irradiance at the detector focal plane. Also needed for this calculation are the absolute peak transmittance values for each filter and the dewar window. These are as follows.

	Absolute Peak Transmittance
2 Quartz windows (0.85 x 2)	0.72
First neutral density filter	0.015
Second neutral density filter	0.015
2 Special black polyethylene filters	$(0.52)^2$
Atmospheric water vapor	0.88

Total transmittance, $T'_R = 3.85 \times 10^{-5}$

A transmittance factor for atmospheric water vapor was also included. Although this produces a small effect on total transmittance, it was found to be not negligible. The effect of atmospheric absorption was checked by flushing the space between the blackbody opening and the dewar window with dry nitrogen. This produced an increase in a Ge:Ga detector's signal by 13%. Since it was impractical to continue flushing this space during all tests, the atmospheric correction factor was applied to the blackbody irradiance calculation.

The equation for signal irradiance, Equation (6) in Section 5, was written as

$$H_{BB}(\Delta\lambda) = \frac{W_{BB}(\Delta\lambda)\, A_{BB}\, T'_R F}{\pi D^2} \qquad \text{(A1)}$$

Substituting the values calculated above, along with those other values listed in Table 5-1, gives

$$H_{BB}(\Delta\lambda) = \frac{(3.29 \times 10^{-4})(7.85 \times 10^{-3})(3.85 \times 10^{-5})(0.4)}{(3.14)(9.58)^2} = 1.38 \times 10^{-13} \text{ w/cm}^2.$$

The background photon flux density at the detector plane was calculated in a similar manner. Column 7 of Table A-1 lists 300°K photon flux density values for each spectral interval as obtained from a radiation slide rule. Column 8 gives the effective values passing through the filter (column 2 × 7) and their sum over all the spectral intervals.

Equation (5) in Section 5 was then used to calculate the background photon flux density at the detector plane. This equation is

$$Q_B(\Delta\lambda) = Q(300°K, \Delta\lambda)\, T_R \sin^2 \theta/2. \qquad (A2)$$

The filter transmittance factor in this case does not include the outer warm quartz window nor does it include the atmospheric water vapor loss. It includes just the two neutral density filters and the two special polyethylene filters. Thus $T_R = 6.1 \times 10^{-5}$. Using this value along with the appropriate values from Tables A-1 and 5-1 gives

$$Q_B(\Delta\lambda) = (1.49 \times 10^{17})(6.1 \times 10^{-5})\left(\frac{0.05}{9.58}\right)^2 = 2.48 \times 10^8 \text{ ph/sec/cm}^2.$$

Ge:Be TEST DEWAR

The Ge:Be Detectors were tested using a 15- to 20.5-μm multilayer band-pass filter plus neutral density filters on germanium. The relative transmittance curve for this band-pass filter is shown in Figure A-2. The blackbody signal irradiance through this filter was calculated by numerical integration in the same manner as was described for the case of Ge:Ga. Table A-2 lists the relevant data.

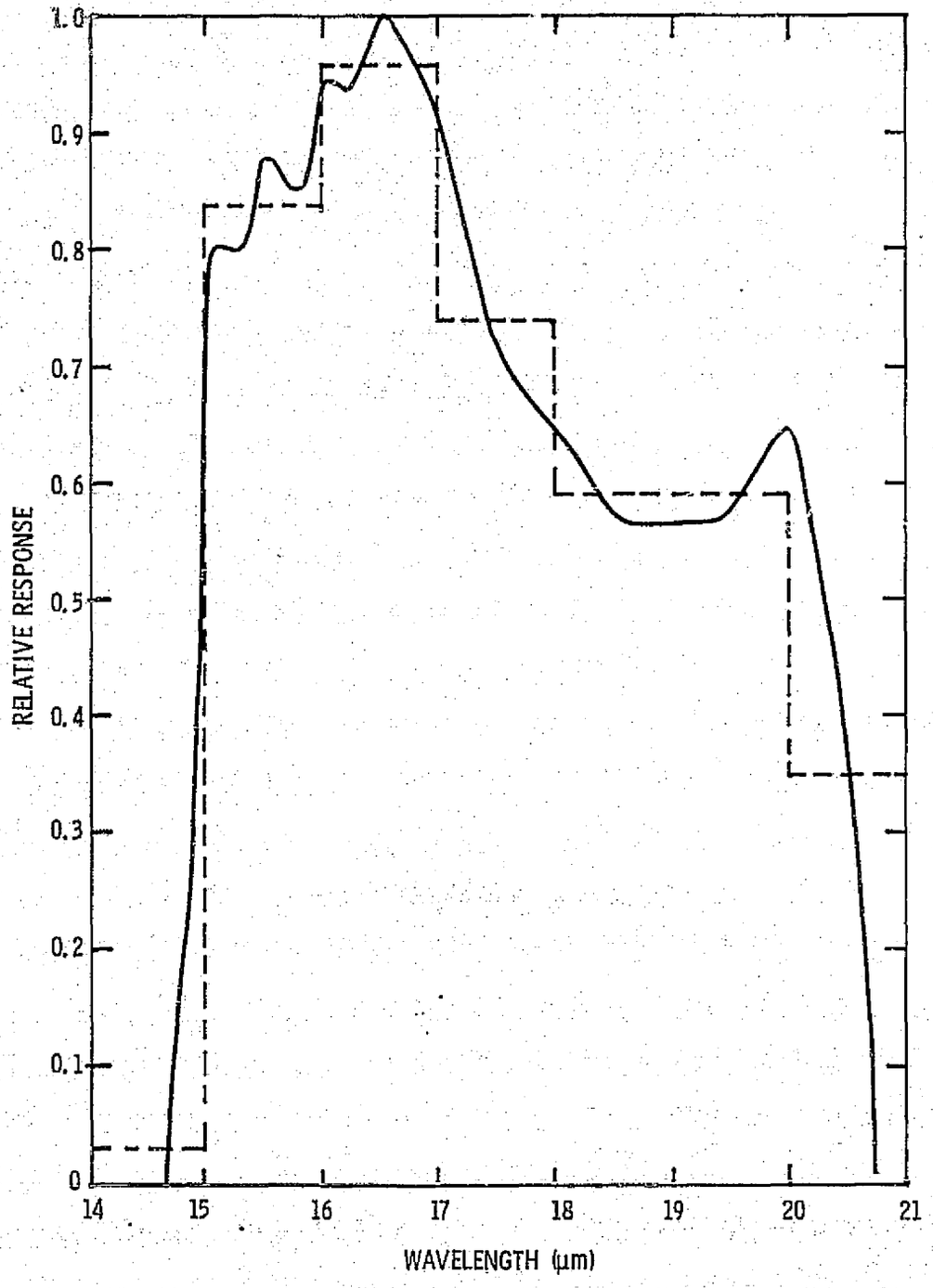

Figure A-2. Relative Spectral Response of Ge:Be Detector with Band-Pass Filter

Table A-2. Listing by Spectral Interval of Blackbody Signal Radiant Emittance and Background Photon Flux Values Used for Ge:Be Detector Testing

(1) λ (μm)	(2) $R_F(\lambda)$	(3) $W_{500}(\lambda)$ (w/cm^2)	(4) $W_{300}(\lambda)$ (w/cm^2)	(5) $W_{500}(\lambda) - W_{300}(\lambda)$ (w/cm^2)	(6) $W_{BB}(\lambda)$ (w/cm^2)	(7) $Q_{300}(\lambda)$ (ph/sec/cm^2)	(8) $Q_B(\lambda)$ (ph/sec/cm^2)
		x 10^{-3}	x 10^{-3}	x 10^{-3}	x 10^{-3}	x 10^{17}	x 10^{17}
14-15	0.03	9.70	2.20	7.50	0.23	1.56	0.05
15-16	0.84	7.70	2.20	5.50	4.62	1.56	1.31
16-17	0.96	6.30	1.75	4.55	4.37	1.44	1.38
17-18	0.74	5.25	1.52	3.73	2.76	1.40	1.04
18-19	0.59	4.55	1.38	3.17	1.87	1.31	0.77
19-20	0.59	3.85	1.29	2.56	1.51	1.23	0.73
20-21	0.35	3.50	1.10	2.40	0.84	1.15	0.40
SUMMATION				$W_{BB}(\Delta\lambda)$ =	1.62×10^{-2}	$Q_B(300, \Delta\lambda)$ =	5.68×10^{17}

Using the data from Tables A-2 and 5-1, and substituting into Equation (A1) gives

$$H_{BB}(\Delta\lambda) = \frac{(1.62 \times 10^{-2})(7.85 \times 10^{-3})(1.47 \times 10^{-4})(0.4)}{(3.14)(8.59)^2} = 3.22 \times 10^{-11} \text{ w/cm}^2.$$

The background photon flux density at the detector was obtained by substituting data from Tables A-1 and 5-1 into Equation (A2) to get

$$Q_B(300°K, \Delta\lambda) = (5.68 \times 10^{17})(2.4 \times 10^{-4})\left(\frac{0.5}{8.59}\right)^2 = 4.6 \times 10^9 \text{ ph/sec/cm}^2.$$

DETECTOR RESPONSIVITY

The blackbody signal irradiance values calculated in this appendix were used to obtain detector responsivity by the usual formula

$$R_v(\lambda) = \frac{V_S(\Delta\lambda)}{H_{BB}(\Delta\lambda)\, A_D} \tag{A3}$$

where $R_v(\lambda)$ is the responsivity in volts/watt, $V_S(\Delta\lambda)$ is the measured signal voltage, A_D is the detector sensitive area, and $H_{BB}(\Delta\lambda)$ is the effective signal irradiance. It turns out that this procedure yields the responsivity at the peak of the filter spectral distribution λ_p. A derivation of this result is as follows.

If $R_v(\lambda)$ is the detector responsivity at any wavelength and $P\lambda$ is the signal power per unit of wavelength (watts/μm) on the detector at this wavelength, then for a given wavelength range between λ_1 and λ_2, the detector signal voltage will be given by

$$V_S(\Delta\lambda) = \int_{\lambda_1}^{\lambda_2} R_v(\lambda)\, P\lambda\, d\lambda \tag{A4}$$

where $\Delta\lambda$ refers to the spectral interval $\lambda_1 - \lambda_2$.

If the detector's $R_v(\lambda)$ curve is expressed as a relative response normalized to unity as shown in Figures A-1 and A-2, then equation (A4) can be written as

$$V_S(\Delta\lambda) = R_v(\lambda_p) \int_{\lambda_1}^{\lambda_2} RR(\lambda)\, P_\lambda\, d\lambda \qquad (A5)$$

where $RR(\lambda)$ is the relative response (= 1 at λ_p) and $R_v(\lambda_p)$ is the responsivity at λ_p. This equation can be rewritten as

$$R_v(\lambda_p) = \frac{V_S(\Delta\lambda)}{\int_{\lambda_1}^{\lambda_2} RR(\lambda)\, P_\lambda\, d\lambda} \qquad (A6)$$

The integral in the denominator is the same as $H_{BB}(\Delta\lambda)\, A_D$ when $H_{BB}(\Delta\lambda)$ is calculated by the numerical integration method described previously in this Appendix. Therefore, the responsivity calculated from equation (A3) is the responsivity at the peak of the relative spectral response curve λ_p.

Appendix B
DETECTOR RESISTANCE MEASUREMENTS THROUGH MOSFET

This appendix describes the method used for determining detector resistance values when the detector is connected to the cryogenic MOSFET source follower preamplifier.

The circuit diagram is shown in Figure B-1. The detector dc resistance is given by

$$R_{dc} = V_D/I \tag{B1}$$

where

$$I = V_B/(R_L + R_{dc}). \tag{B2}$$

The voltage drop across the detector V_D will appear at the MOSFET source terminal multiplied by the gain of the source follower. This voltage is measured by observing the change in V_S as the detector bias voltage is switched from zero to ON. Thus,

$$V_D = \Delta V_S/0.85 \tag{B3}$$

where ΔV_S is the observed charge in source voltage and 0.85 is the source follower gain. Combining equations (B1), (B2) and (B3) gives

$$R_{dc} = \frac{R_L}{\left(\frac{0.85\ V_B}{\Delta V_S}\right) - 1} \tag{B4}$$

Use of this equation requires prior knowledge of the load resistance R_L. Since the load resistance value can vary with temperature and bias voltage, this may introduce considerable error into the determination of R_{dc} by this method. Values of V_B and ΔV_S can be measured with good precision and will not produce a large error.

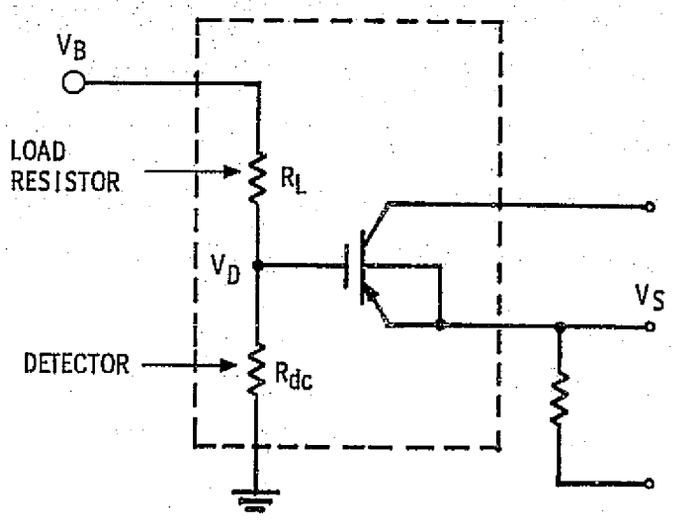

V_B = BIAS VOLTAGE APPLIED EXTERNALLY ACROSS BOTH DETECTOR AND LOAD

V_D = VOLTAGE DROP ACROSS DETECTOR

V_S = SOURCE VOLTAGE

Figure B-1. Circuit Diagram for Low-Background Detector Testing

Table B-1 shows measured resistance values versus temperature and applied voltage for a typical load resistor used in the detector assemblies delivered on this program. It is clear from these data that good calibration of the load resistor must be accomplished to obtain accurate values for R_{dc} from equation (B4).

Table B-1. Resistance Versus Temperature of Typical Load Resistor Used in IRAS Device Assemblies

Temperature (°K)	Resistance (Ω) at 0.020 V	Resistance (Ω) at 0.200 V	Resistance (Ω) at 2.00 V
4.2	3.8×10^{10}	3.7×10^{10}	2.7×10^{10}
4.0	3.7×10^{10}	3.9×10^{10}	2.8×10^{10}
3.5	4.4×10^{10}	4.7×10^{10}	3.2×10^{10}
3.0	5.1×10^{10}	6.0×10^{10}	3.7×10^{10}

Another obvious method for determining R_{dc} would be to attach an additional wire to the detector at the connection to the MOSFET gate and bring this lead out of the dewar. Measurements of detector current and voltage could then be made directly. However, two problems arise with this method. First, the additional lead to the detector produces an added capacitance at the gate input which will cause the circuit response to roll off at lower frequencies. Since the combination of MOSFET gate input and detector capacitance is only about 5 pf, distributed capacitance from the additional wire could easily equal or exceed this value. Secondly, the insulation resistance of the dewar feed-throughs has to be very high; in fact, much higher than the detector resistance. If detector resistance values are in the 10^{10}-ohm range, the insulator resistance should be greater than 10^{12} ohms. The metal-glass feed-throughs used on our dewars can have this high an insulation resistance if properly cleaned and kept dry. However, past experience has shown that they are easily contaminated with use and leakage problems result. It was because of these problems that the indirect method of detector resistance measurement described above was adopted.